Colloquium: Topologically protected transport in engineered mechanical systems

Tirth Shah*

Max Planck Institute for the Science of Light, Staudtstrasse 2, 91058 Erlangen, Germany and Department of Physics, Friedrich-Alexander Universität Erlangen-Nürnberg, Staudtstrasse 7, 91058 Erlangen, Germany

Christian Brendel and Vittorio Peano

Max Planck Institute for the Science of Light, Staudtstrasse 2, 91058 Erlangen, Germany

Florian Marquardt

Max Planck Institute for the Science of Light, Staudtstrasse 2, 91058 Erlangen, Germany and Department of Physics, Friedrich-Alexander Universität Erlangen-Nürnberg, Staudtstrasse 7, 91058 Erlangen, Germany

(published 18 April 2024)

Mechanical vibrations are being harnessed for a variety of purposes and at many length scales, from the macroscopic world down to the nanoscale. The considerable design freedom in mechanical structures allows one to engineer new functionalities. In recent years, this has been exploited to generate setups that offer topologically protected transport of vibrational waves (topological phonon transport), both in the solid state and in fluids. Borrowing concepts from electronic physics and being cross fertilized by concurrent studies for cold atoms and electromagnetic waves, this field of topological transport in engineered mechanical systems offers a rich variety of phenomena and platforms. In this Colloquium, a unifying overview of the various ideas employed in this area is provided, different approaches and experimental implementations are summarized, and the challenges as well as the prospects are commented upon.

DOI: 10.1103/RevModPhys.96.021002

CONTENTS

I. INTRODUCTION

Topology is a branch of mathematics that deals with properties of objects that are invariant under smooth deformation. Even in the earliest days of research in topology, potential connections to physics were already pointed out. In the 1860s, for example, Lord Kelvin speculated that atoms might be knots in the ether, and this inspired the first attempts at a complete classification of knots. While this idea was not borne out, topological defects are now known to occur in a large variety of important physical settings, ranging from vortices in fluids and superfluids and dislocations in crystalline solids to liquid crystals as well as magnetic skyrmions. Even on the largest scales, topological defects may play a role in the form of cosmological strings.

These are all examples of topology directly present in real-space structures. A more subtle but far-reaching example of topological physics was uncovered upon closer inspection of the quantum Hall effect, pointing toward topological properties of Bloch waves in quasimomentum space. After its discovery in 1980 (Klitzing, Dorda, and Pepper, 1980), the surprising precision of the quantization of Hall resistance in a 2D electron sample in a magnetic field (even in the presence of

*tirth.shah@mpl.mpg.de

disorder) called for a fundamental explanation. An early explanation given by Laughlin (1981) was at its heart a topological argument. However, the entirety of the deep connection to mathematical topology was uncovered a bit later, when Thouless *et al.* (1982) and Kohmoto (1985) showed that the quantized Hall conductance is directly related to a topological invariant, the so-called Chern number. This invariant can be calculated for an infinitely extended periodic system where it relates to how the Bloch waves change when moving through quasimomentum space.

In general, topological invariants, i.e., quantities that do not change under smooth deformations, play a prominent role in any analysis of topology. Simple examples include winding numbers for vortices and the number of holes in an object. While the Chern number can be calculated for the infinitely extended bulk system, it is directly related to the number of edge channels that carry electrical current along the boundary of a finite sample. This is the bulk-boundary correspondence. These edge channels are topologically protected against backscattering, which explains the precision of conductance quantization even in the presence of disorder.

Haldane (1988) showed that it is the breaking of time-reversal symmetry, and not a finite magnetic field, which is responsible for nonzero Chern numbers and the unidirectional edge channels, leading to a general discussion of so-called Chern insulators. Later Kane and Mele (2005a) and Bernevig and Zhang (2006) pointed out that it is possible to obtain topological transport even for time-reversal-invariant systems, introducing the study of topological insulators. In such materials, the intrinsic spin-orbit coupling leads to spin-polarized unidirectional edge channels (so-called "helical" channels). This phenomenon is now called the quantum spin Hall effect. A review of these developments was given by Hasan and Kane (2010).

Given the importance of topologically protected transport in the domain of electronic systems, it was natural to ask whether other systems could show the same kind of physics. However, this raised a number of challenges since many interesting particles and excitations neither are affected by magnetic fields nor naturally exhibit some kind of spin-orbit coupling. This pertains to cold atoms as well as photons and phonons. In all of these cases, some engineering is required to make progress toward the realization of topological transport.

The first ideas for the design of artificial magnetic fields for neutral particles emerged in the field of cold atoms in optical lattices (Jaksch and Zoller, 2003). A few years later, the breaking of time-reversal symmetry for microwave photons using the magneto-optical effect as a means of producing chiral edge channels was suggested and subsequently realized (Haldane and Raghu, 2008; Wang *et al.*, 2009). Since those days, considerable progress has been made in the design and exploitation of artificial chiral transport in cold atomic systems (Aidelsburger, Nascimbene, and Goldman, 2018; Cooper, Dalibard, and Spielman, 2019) and photonic systems (Lu, Joannopoulos, and Soljačić, 2014; Ozawa *et al.*, 2019).

In this Colloquium, we devote our attention to another important excitation: phonons, i.e., vibrations in solids or sound waves in fluids. The topological waves of interest here need not to be quantized, but we, like many researchers in the field, still use the terminology *phonons* even when referring to high-amplitude, classical vibrations involving many phonons. Just as with photons and neutral cold atoms, the basic underlying mathematics is the same as that for electrons. This shared language across platforms has proven to be beneficial, as it has enabled researchers to learn from ideas first advocated for in other settings and adapt them in a suitable manner. However, despite this joint basis there are important differences that make every platform unique with its own challenges and opportunities. For example, the design capabilities, the readout modalities, and the possibilities of creating excitations and of coupling them to other systems are all vastly different, in addition to the large range in physical parameters. More specifically, for phononic systems their technological application potential is greatly aided by the compactness of the resulting devices when they are fabricated in the form of nanomechanical systems (Bachtold, Moser, and Dykman, 2022). This is due to the relatively slow wave speed, which allows for devices that are a million times smaller than photonic systems at the same frequencies. As a solid-state platform for quantum technologies, they also offer unique efficient coupling to localized spins and other solid-state qubits (like superconducting qubits or quantum dots) (Safavi-Naeini *et al.*, 2019; Clerk *et al.*, 2020; Barzanjeh *et al.*, 2022). This could turn topologically protected phononic edge channels into a particularly promising way of interconnecting such qubits or quantum sensors (Lemonde *et al.*, 2019). We add that optomechanical interactions (Aspelmeyer, Kippenberg, and Marquardt, 2014; Barzanjeh *et al.*, 2022; Delaney *et al.*, 2022) represent one of the most promising ways to turn on-chip quantum information into photons for long-distance communication, adding to the power of on-chip phononic networks. All of these are reasons for studying the topologically protected transport of phonons. Ideas like unidirectional amplification inside chiral edge channels (Peano *et al.*, 2016) add to these prospects.

As we describe in this Colloquium, the design of vibrational topological transport started in the macroscopic domain, including pendula and sound waves in flowing fluids, but is now moving into the microscopic and nanoscopic domains, reaching important milestones such as detection precision at the scale of thermal fluctuations (Ren *et al.*, 2022), gigahertz carrier frequencies (Zhang *et al.*, 2022), and submicron lattice constants (Nii and Onose, 2023). This ongoing progress in miniaturization will unlock the aforementioned promising applications.

In this Colloquium, we concentrate on topologically protected transport along phononic edge channels since that is the most promising area for applications. This means that we deal here specifically with 1D edge channels at the boundary of 2D systems (which in the nanoscopic domain are engineered chip platforms). There are other interesting aspects of phonon topology that we do not cover, like zero-frequency modes in isostatic lattices (Kane and Lubensky, 2014), 0D localized states [for example, at the boundary of the 1D Su-Schrieffer-Heeger model (Xiao, Ma *et al.*, 2015; Yang and Zhang, 2016; Chaunsali *et al.*, 2017) or in the form of corner states (Serra-Garcia *et al.*, 2018) or Dirac vortices (Ma *et al.*, 2021)], and Weyl cones in 3D systems (Xiao, Chen *et al.*, 2015; Yang and Zhang, 2016; Fruchart *et al.*, 2018; Ge *et al.*, 2018; He *et al.*, 2018; Li *et al.*, 2018; Wang and Tsai, 2018). Some reviews on

phononic topology already exist (Huber, 2016; Zhang, Xiao *et al.*, 2018; Ma, Xiao, and Chan, 2019; Liu, Chen, and Xu, 2020; Nassar *et al.*, 2020; Huang, Chen, and Huo, 2021; Miniaci and Pal, 2021) but have a different scope than our work: Huber (2016) and Ma, Xiao, and Chan (2019) offered short reviews of the field, Zhang, Xiao *et al.* (2018) covered acoustic systems, Miniaci and Pal (2021) and Huang, Chen, and Huo (2021) discussed elastic systems, while Nassar *et al.* (2020) focused mainly on nonreciprocal systems. In this Colloquium, we present an up-to-date snapshot of the field, covering a wide variety of systems including both acoustic- and elastic-wave systems, as well as discrete mechanical systems like arrays of gyroscopes and pendula. We also give a comprehensive and unifying discussion of the physics behind the different design possibilities, emphasizing the conceptual connections and differences between the various design schemes. Finally, we analyze the peculiarity of mechanical waves compared to other types of topological waves and the challenges hampering future applications.

Our Colloquium is organized as follows: We first describe the general platform-independent mathematics behind topologically protected transport: topology in band structures, the bulk-boundary correspondence, Chern numbers in systems with broken time-reversal symmetry, and topological insulators with intact time-reversal symmetry. We then provide an overview of the entire field of topological phonon transport, highlighting the general trends and some early works in this domain. The bulk of this Colloquium is given in Sec. IV. There we discuss in more detail the similarities and differences among electrons, electromagnetic waves, and vibrations in the context of topological transport. We then describe each of the different approaches to designing topological transport: from engineering the breaking of time-reversal symmetry, thus leading to phononic Chern insulators, to the various design schemes that rely purely on suitable geometry and connectivity and do not require broken time-reversal symmetry. We conclude with a discussion of challenges, like mechanical dissipation, and future applications.

II. GENERAL BACKGROUND: TOPOLOGICAL TRANSPORT OF WAVES

A. Overview: Topology in band structures and bulk-boundary correspondence

In mathematics, topological properties of geometrical objects are those that are invariant under smooth deformations, such as the number of holes in the object. Even before the discussion of topological transport, the existence of topological features in physics had long been recognized. Early examples include topological defects in fields (Mermin, 1979), such as vortices and skyrmions. Mathematically a continuous deformation of one function (for example, a field) into another function (a smoothly distorted version of the field) is denoted as a "homotopy" and establishes that the two functions are topologically equivalent.

When we turn to the propagation of waves in an infinitely extended 2D periodic medium [Fig. 1(a)], we arrive at the concept of Bloch waves as stationary solutions of the underlying wave equation. Attention often tends to be focused on

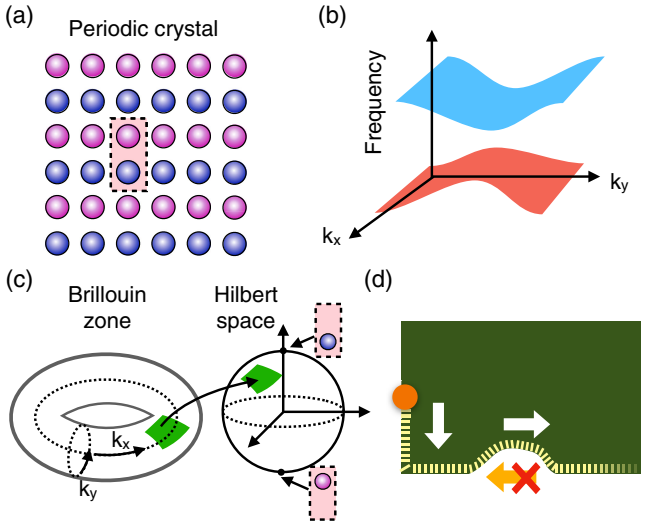

FIG. 1. Topological transport. (a) Schematic of a periodic crystal with two different sublattices. (b) Fictitious band structure of (a) featuring two bands with a band gap in the middle. (c) Topological features can be inspected by investigating, for each band, the map from the Brillouin zone (torus) to the Hilbert space. Here it is visualized as a Bloch sphere. Each pole represents a Bloch wave localized on a sublattice. (d) Topologically protected edge state featuring transport in only one direction (for a Chern insulator). The transport is immune to backscattering even at irregularities.

the band structure, i.e., the eigenfrequencies of these waves as a function of their quasimomentum inside the Brillouin zone; cf. Fig. 1(b). However, to discover topological features, one needs to inspect the behavior of the Bloch waves themselves. The Brillouin zone is formally equivalent to a torus, i.e., a compact manifold. The Bloch waves live in a Hilbert space of suitably normalized wave functions, again a compact manifold. One can thus ask what happens to this map [see Fig. 1(c)] from Brillouin zone to Hilbert space when the underlying periodic medium is smoothly deformed (for example, when changing the geometry or potential), and thereby arrive at topological properties. These properties, typically expressed via so-called topological indices, remain invariant as long as the smooth deformations leave the map uniquely defined. This breaks down only when a band gap closes, leading to a degeneracy at some point in the Brillouin zone. This is when topological properties can change abruptly.

Studying these topological properties by inspecting Bloch waves in the bulk can be done mathematically but is rather difficult in experiments since it requires measurement access to the wave functions (Li *et al.*, 2016). However, one of the most noteworthy aspects of Bloch-wave topology is that the mathematical properties of the bulk have immediate consequences for what happens at the boundary of a finite sample, or at an interface between two domains of the medium that have different topological features. In particular, lower-dimensional stationary states develop at the boundary or interface, the so-called edge states; cf. Fig. 1(d). This is the bulk-boundary correspondence. It is these edge states that permit topologically protected robust transport and that are of greatest importance for potential applications.

We now review the more detailed description of edge states and bulk topological indices. Two qualitatively different situations have to be distinguished, according to whether time-reversal symmetry is broken or not. For the time-symmetric case, we further distinguish between the schemes that allow one to implement a spin-Hall Hamiltonian supporting spin Chern numbers for each of two local phononic pseudospin directions, and those in which each pseudospin direction and the corresponding topological excitations are described by a Dirac Hamiltonian derived within a smooth-envelope approximation. While our description should be sufficient to provide the reader with enough background to be able to understand the remainder of this Colloquium, with the applications to topological transport in mechanical systems there are much more extensive mathematically oriented reviews that can be consulted for additional details (Hasan and Kane, 2010; Ozawa *et al.*, 2019).

B. Broken time-reversal symmetry

The topological properties of interest in the general field of topological band structures are properties of a band gap that are invariant under continuous modifications of the underlying Hamiltonian. As discussed, these properties are encoded in so-called topological invariants, integer quantities that are a function of the bulk normal modes but that can also be inferred directly from the spectrum in a system with a physical boundary. Here we highlight this aspect for the special case of systems with broken time-reversal symmetry. For this purpose, we initially consider the simplest geometry comprising a physical boundary: a semi-infinite plane [Fig. 2(a)]. This approach also provides some simple physical intuition for the resulting topologically robust transport and to understand why a $\mathbb{Z}$-topological invariant (assuming arbitrary integer values) is required to classify topological band gaps in systems with broken time-reversal symmetry.

For a semi-infinite plane, the frequency can be plotted as a function of the quasimomentum in the direction longitudinal to the edge, which is a conserved quantity. A typical example of such a band structure is shown in Fig. 2(b). In this example, two blue (dark gray) bulk bands separated by a green (light gray) bulk band gap are connected via a gapless edge state. The edge state is a right mover because the slope, which sets the group velocity, is always positive [Figs. 2(a) and 2(b)]. The chiral nature of the wave transport is robust even when weak disorder (compared to the width of the bulk band gap) is introduced into the system: no backscattering can occur, simply because the system does not support any left-moving states in the bandwidth of interest. This argument applies even when the edge changes direction at a corner in a finite system with a closed boundary [Fig. 2(d)]. We note that the breaking of time-reversal symmetry is a precondition to realize this kind of physics because it opens up the possibility of engineering systems with chiral edge states without time-reversed counter-propagating solutions.

Next we consider any arbitrary translationally invariant continuous modification of the underlying Hamiltonian that does not close the bulk band gap. The band structure will then also change continuously, with the only constraint being that the edge bands should remain single-valued periodic functions

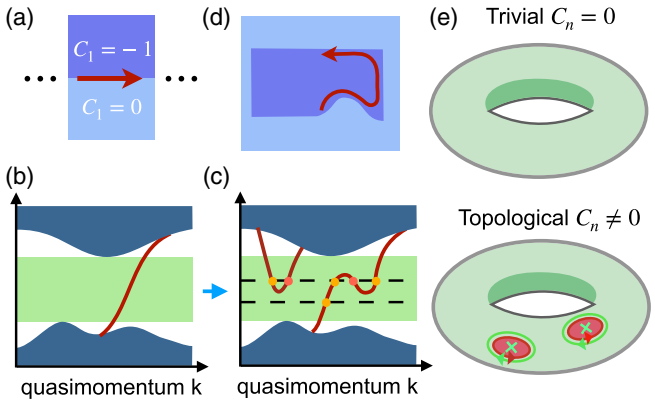

FIG. 2. Topological transport in a Chern insulator. (a) Domain-wall geometry. Also indicated are the Chern number of the lower band for the two domains and the edge-state propagation direction (arrow). (b) Topological band structure for the domain-wall geometry shown in (a). (c) Band structure of a smoothly deformed system, with the same resulting net number of right movers at any frequency. (d) Robustness against deformations of the domain wall. (e) Global properties of the Berry connection. The shade of green (gray) identifies a BZ region over which $\mathcal{A}_n(\mathbf{k})$ varies smoothly. Each region is defined by fixing the phase of the Bloch waves on a particular sublattice. For the topological case, the crosses indicate quasimomenta whose Bloch waves have zeros at the sublattice used to define the gauge in the light-shaded region.

of the quasimomentum or start from a bulk band and end in the neighboring bulk band (such edge bands would also be periodic functions of the quasimomentum in a strip configuration with a finite number of bands). For example, conceivable continuous modifications could introduce one or more local maxima in the edge band or pull one or more edge bands into the bulk bands; cf. Fig. 2(c). We observe that these modifications might lead to a frequency-dependent number of edge states also giving rise to left-moving states. However, no conceivable continuous modification can change the difference of the numbers of right movers and left movers without closing the bulk band gap. Thus, the net number of edge states $N_R - N_L$ (with N_R and N_L the number of right and left movers, respectively) is a $\mathbb{Z}$-topological invariant. Here $\mathbb{Z}$ indicates that the invariant takes an arbitrary integer value.

The net number of edge states has its foundation in the topological properties of the bulk of the system. Indeed, it is fixed by the bulk-boundary correspondence (Hatsugai, 1993; Bernevig and Hughes, 2013; Asbóth, Oroszlány, and Pályi, 2016; Prodan and Schulz-Baldes, 2016) $N_R - N_L = -\sum_n C_n$, where the sum is taken over the bands below the band gap of interest and the band's Chern number C_n is an integer-valued global property of the band's Bloch waves across the Brillouin zone (BZ) (Thouless *et al.*, 1982). In a two-material scenario in which a domain wall separates two domains with different bulk Hamiltonians, the same formula holds, with the difference being that Chern numbers across the surface replace the Chern number.

As originally recognized by Simon (1983), the Thouless–Kohmoto–Nightingale–den Nijs invariant (Thouless *et al.*,

1982), later known as the Chern number, can be defined as a surface integral of a curvature

$$C_n = \frac{1}{2\pi}\int_{\mathrm{BZ}} d^2k[\nabla_{\mathbf{k}} \times \mathcal{A}_n(\mathbf{k})]\cdot \mathbf{e}_z. \tag{1}$$

The relevant surface (the BZ) is a torus and the curvature (known as the Berry curvature) is the curl of the Berry connection $\mathcal{A}_n(\mathbf{k}) = i\langle \mathbf{k}_n|\nabla_{\mathbf{k}}|\mathbf{k}_n\rangle$, where $|\mathbf{k}_n\rangle$ are the Bloch waves for the nth band. We note that the Berry connection $\mathcal{A}_n(\mathbf{k})$ plays a role similar to the vector potential in electromagnetism. Here too Stokes's theorem allows one to convert surface integrals into line integrals over the surface boundary, which can be interpreted as the geometrical Berry phases (Berry, 1984) accumulated while the quasimomentum is adiabatically varied along a closed path. For a trivial band, one can define a Berry connection $\mathcal{A}_n(\mathbf{k})$ that varies smoothly across the BZ by fixing the phase of all Bloch waves at the same sublattice. This allows one to apply Stokes's theorem to the BZ as a whole and conclude that the Chern number is zero, as the BZ has no boundary; cf. Fig. 2(e) (top sketch). For a topological band [bottom sketch of Fig. 2(e)], it is not possible to fix a global gauge in this manner, because for any choice of sublattice there are one or more quasimomenta (crosses) whose Bloch waves have a zero (Kohmoto, 1985). In the neighborhoods of a zero (the dark patches), one can fix the phase at a different sublattice. This leads to a phase mismatch $f(\mathbf{k})$ between the Bloch waves inside and immediately outside of a patch: $|\mathbf{k}_n\rangle$ inside the patch (on the dark contours) is transformed into $\exp[if(\mathbf{k})]|\mathbf{k}_n\rangle$ outside (the light contours). The phase mismatch must increase by a multiple of 2π while moving in a circle along a patch boundary, defining a winding number for the patch. By applying Stokes's theorem separately to each patch and to the region outside of the patches (the light-shaded region), one can show that the Chern number is simply the sum over the patches of the patch winding numbers (Kohmoto, 1985; Ohgushi, Murakami, and Nagaosa, 2000).

C. Time-reversal-symmetric topological insulators

1. Edge states protected by Kramers degeneracy

Time-reversal symmetry significantly constrains the topological properties of 2D systems. For each finite-speed boundary excitation in the bulk band gap of an insulator, there should be a counterpropagating time-reversed partner. This also means that the sum of the Chern numbers for the bands below a band gap is always zero (Brouder *et al.*, 2007). Nevertheless, boundary excitation of time-reversal-symmetric systems can have a topological underpinning, as originally predicted (Kane and Mele, 2005a; Bernevig and Zhang, 2006) and experimentally demonstrated (König *et al.*, 2007) in electronic systems. The topological protection for these types of edge states results from a general property of fermionic systems. For every normal mode $|\psi\rangle$ there is a time-reversed partner normal mode $\mathcal{T}|\psi\rangle$ with equal frequency. This property, known as Kramers degeneracy, arises because the time-reversal operator $\mathcal{T}$ squares to minus the identity ($\mathcal{T}^2 = -\mathbb{1}$) for any fermionic excitation with half-integer total spin (Landau and Lifshitz, 1981). This implies that the coupling between a "Kramers pair" of time-reversed counterpropagating boundary excitations in the bulk band gap of a topological insulator is forbidden because it would split the degeneracy; cf. Fig. 3(a). This results in transport that is robust against backscattering in the presence of weak time-reversal-symmetric disorder.

Next we show how a topological invariant can be inferred from the spectrum of a system with a semi-infinite geometry. As in the Chern insulator case, we discuss how a band structure can be modified under continuous translationally invariant changes of the underlying Hamiltonian that do not close the bulk band gap, here with the additional prescription that the time-reversal symmetry is preserved. Without loss of information, we display only positive quasimomenta [$E_n(k) = E_n(-k)$ because of the time-reversal symmetry]; cf. Figs. 3(b) and 3(c). For the band structure of a time-reversal-symmetric Hamiltonian with $\mathcal{T}^2 = -\mathbb{1}$, only the band crossings that occur at a time-reversal-invariant high-symmetry point are essential symmetry-protected degeneracies. In a semi-infinite configuration these are the Γ and X points with quasimomenta $k = 0$ and π/a (with a the lattice constant), respectively. Accidental band crossings away from these special quasimomenta are not a consequence of Kramers degeneracy (the underlying normal modes are not Kramers pairs) and can be lifted without breaking the time-reversal symmetry. Starting with any arbitrarily complicated band structure, lifting accidental degeneracies, and pulling edge bands (pairs of edge

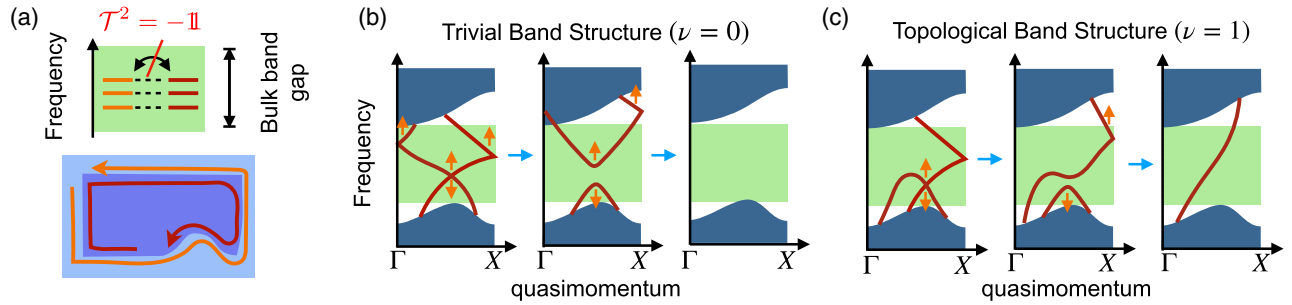

FIG. 3. (a) Top sketch: spectrum of a finite-size time-symmetric topological insulator. Each pair of degenerate levels corresponds to a pair of counterpropagating edge waves (bottom sketch). Any coupling is forbidden because it would violate Kramers degeneracy. (b) Trivial and (c) topological band structures in a semi-infinite plane geometry. The degeneracies at the time-symmetric high-symmetry points Γ and X correspond to Kramers doublets. The trivial and topological band structures, respectively, can be smoothly modified into a gapped band structure and a band structure with a single edge state connecting the two bulk bands without lifting any Kramer doublets.

bands) into the bulk bands, we arrive at either of two topologically distinct configurations: a trivial configuration in which no edge band is present [see Fig. 3(b)] or a topological configuration in which a single edge band connects the bulk bands below and above the band gap [cf. Fig. 3(c)]. Thus, the topology of 2D time-symmetric topological insulators is encoded in a $\mathbb{Z}_2$-topological invariant. Here $\mathbb{Z}_2$ refers to the cyclic group formed by the two possible values of the invariant (Kane and Mele, 2005b). By convention, the value $\nu = 1$ ($\nu = 0$) is assigned to the topological (trivial) configuration.

However, for bosonic excitations and, in particular, the phononic excitations of interest in this Colloquium, the physical time-reversal symmetry squares to the identity $\mathcal{T}^2 = \mathbb{1}$. Thus, Kramers degeneracy does not naturally emerge in the presence of time-reversal symmetry in bosonic systems. Nevertheless, no fundamental principle prevents us from engineering the effective Hamiltonian of a bosonic system identical to the single-particle Hamiltonian of a fermionic system of interest (here a topological insulator). In this scenario, Kramers degeneracy will be produced via an engineered local antiunitary symmetry $\mathcal{T}_{\text{en}}$ with $\mathcal{T}_{\text{en}}^2 = -\mathbb{1}$. We note that $\mathcal{U} = \mathcal{T}_{\text{en}}\mathcal{T}$ is then a local unitary symmetry that can be interpreted as a conserved pseudospin. In practice, the pseudospin can be a duplicate or internal degree of freedom in an array of discrete systems, such as coupled pendula or whispering gallery mode resonators (Sec. IV.C.1). For the special case of a binary pseudospin (equivalent to a spin 1/2 particle), we have

$$\hat{H} = \begin{pmatrix} \hat{H}_\uparrow & 0 \\ 0 & \hat{H}_\downarrow \end{pmatrix}, \tag{2}$$

with $\hat{H}_\downarrow = \hat{H}_\uparrow^*$. For a topological bosonic insulator, each pseudo-spin-polarized block supports arbitrary integer nonzero Chern numbers. An explicit example is given in Sec. IV.C.1. We note that for electronic systems, this form of the quantum spin-Hall Hamiltonian corresponds to the special case in which the out-of-plane mirror transformation is a symmetry. Without this symmetry, a Rashba spin-orbit interaction leads to a coupling of the two blocks (Kane and Mele, 2005a). This more general form can be implemented in a bosonic system only by breaking the physical time-reversal symmetry $\mathcal{T}$. Conversely, any perturbation that couples the different pseudospin directions without breaking $\mathcal{T}$ will break $\mathcal{T}_{\text{en}}$, and thus evade the topological protection.

2. Engineered Dirac Hamiltonians

For continuum systems such as photonic or phononic crystals, it is usually impossible to engineer a desired effective Hamiltonian across the entire BZ. This limitation can be circumvented by designing edge states that remain well localized in quasimomentum space but can nonetheless propagate along arbitrarily shaped domain walls with negligible backscattering, even turning sharp corners; cf. Fig. 4(a). In Sec. IV.C, we review several schemes to engineer such quasi-momentum-localized edge states. These schemes have a common theoretical foundation based on an effective Dirac equation that we review in this section.

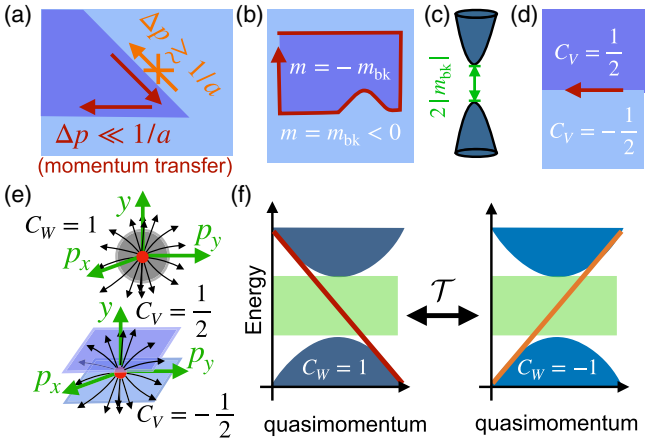

FIG. 4. Edge states generated via an engineered Dirac Hamiltonian. (a) Edge excitations can travel around arbitrarily shaped corners. The change of direction involves only a small momentum transfer Δp. Backscattering requires large Δp and thus is suppressed. (b) Edge channel localized along a domain wall separating two domains governed by the Dirac Hamiltonian Eq. (3) with opposite values $\pm m_{\text{bk}}$ of the mass parameter m. (c) The two domains share the same gapped Dirac-cone band structure. (d) Straight domain-wall geometry. The valley Chern numbers C_V are also indicated. (e) Top sketch: flux C_W of the Berry curvature through a closed surface surrounding the Weyl (Dirac) point (red). The flux lines are shown in black. C_W is equal to the difference of the fluxes through two semi-infinite planes in different domains (bottom sketch) or, equivalently, the difference of the local valley Chern numbers. (f) Band structure for the geometry and chiral charge displayed in (d) and (e) (left sketch) and for the time-reversed Dirac Hamiltonian (right sketch). The edge states obey the bulk-boundary correspondence.

The Dirac equation describes two (out of infinitely many) bands of the continuum system in a restricted bandwidth and quasimomentum region that is often referred to as the valley. It reads (Jackiw and Rebbi, 1976; Semenoff, 1984)

$$\omega\mathbf{\Psi}(\mathbf{x}) = \hat{H}\mathbf{\Psi}(\mathbf{x}), \qquad \hat{H} = \omega_0 + m(\mathbf{x})\hat{\sigma}_z + v\mathbf{p}\cdot\hat{\boldsymbol{\sigma}}, \tag{3}$$

where v is the Dirac velocity, $\hat{\sigma}_{x,y,z}$ are the Pauli matrices, $\hat{\boldsymbol{\sigma}} = (\hat{\sigma}_x, \hat{\sigma}_y)$, and $\mathbf{x} = (x, y)$ and $\mathbf{p} = (-id/dx, -id/dy)$ are the position and momentum variables, respectively. The mass function $m(\mathbf{x})$ assumes opposing values $m(\mathbf{x}) = \pm m_{\text{bk}}$ in two distinct bulk regions divided by a one-dimensional zero-mass domain wall; cf. Fig. 4(b). In this way, the two bulk regions share the same gapped Dirac-cone band structure; cf. Fig. 4(c). We note that formally $\mathbf{p} \in \mathbb{R}^2$, as in a system without an underlying bulk crystal structure. This reflects the fact that the lattice has been eliminated under the assumption that the envelope wave function $\mathbf{\Psi}(\mathbf{x})$ is smooth on the lattice length scale. Thus, the Dirac equation will provide reliable results only if $|\mathbf{p}| \lesssim 1/a$.

Before providing more details on the derivation and limit of validity of the Dirac equation, we discuss its topological properties when it is taken at face value (i.e., without viewing it as only an approximation in a small region of quasimomentum space). For a straight domain wall (for concreteness

in the x direction), the Dirac equation supports the edge band $\omega = \mathrm{sgn}(m_{\mathrm{bk}})vp_x$ with envelope wave function

$$\mathbf{\Psi}(\mathbf{x}) = \begin{pmatrix} 1 \\ \mathrm{sgn}(m_{\mathrm{bk}}) \end{pmatrix} e^{ip_x x} e^{\mathrm{sgn}(m_{\mathrm{bk}})\int_0^y m(y')dy'/v}. \tag{4}$$

In Eq. (4) m_{bk} is the mass in the lower-half plane; cf. Figs. 4(d) and 4(f). This solution, which was originally derived by Jackiw and Rebbi (1976), connects the lower and upper bulk bands. Additional edge states starting and ending in the same bulk band can also appear for a smooth $m(y)$; see Wang *et al.* (2020). In any case, a smooth deformation of $m(y)$ that does not eliminate the domain wall preserves the net number of edge states,

$$N_R - N_L = \mathrm{sgn}(m_{\mathrm{bk}}). \tag{5}$$

This topological feature has its underpinning in a spectral-flow theorem recently introduced by Faure (2022) for topological waves in continuum systems without an underlying bulk crystal symmetry, like ocean waves (Delplace, Marston, and Venaille, 2017; Faure, 2022) and plasma waves (Qin and Fu, 2023). Faure's theory treats the coordinate y transverse to a domain wall as an auxiliary momentum. In this setting, the Dirac point can be viewed as a Weyl point in the three-dimensional space $\mathbf{p}_{3\mathrm{D}} = (p_x, p_y, y)$. Faure's theorem applied to the Dirac equation relates the flux C_W of the Berry curvature through a closed surface surrounding the Weyl point to the net number of edge states $N_R - N_L = -C_W$. From the theory of Weyl semimetals, it is well known that Weyl points are "monopoles" for the Berry curvatures with "chiral charge" $C_W = -\mathrm{sgn}(m_{\mathrm{bk}})$ (Wan *et al.*, 2011). Thus, we recover Eq. (5), giving it a topological interpretation. We note that for the Dirac equation Faure's theorem can be cast in the form of a bulk-boundary correspondence $N_R - N_L = -\Delta C$, where ΔC is the difference between the valley Chern numbers across the domain wall; cf. Fig. 4(e). In each bulk region, the valley Chern number C_V is defined as in Eq. (1) but now integrated over the p_x-p_y plane instead of the BZ: $C_V = \mathrm{sgn}(m)/2$ (Zhang, MacDonald, and Mele, 2013).

Next we discuss the applicability of the Dirac equation to time-reversal-invariant systems. We observe that the Dirac Hamiltonian (3) is not invariant under any antiunitary symmetry $\mathcal{T}$ (with $\mathcal{T}^2 = 1$). For this reason, Dirac cones must always appear in pairs in time-symmetric systems. It is possible to describe each cone with a copy of Eq. (3). Because of the time-reversal symmetry, the two copies must have opposing mass parameters. This ensures that the two Dirac Hamiltonians also have opposing chiral charges C_W, and thus the domain wall supports counterpropagating edge states; cf. Fig. 4(e). Introducing a binary valley pseudospin degree of freedom $\tau_z = \pm 1$, we arrive at the effective Hamiltonian

$$\hat{H} = \omega_0 + m(\mathbf{x})\hat{\tau}_z\hat{\sigma}_z + v\mathbf{p}\cdot\hat{\boldsymbol{\sigma}}. \tag{6}$$

We note that this is equivalent to the large-wavelength limit of the Bernevig-Hughes-Zhang model (Bernevig, Hughes, and Zhang, 2006), a well-known model for topological insulators. In addition to the time-reversal operator $\mathcal{T} = \hat{\tau}_y\hat{\sigma}_y\mathcal{K}$, it also supports an antiunitary symmetry $\mathcal{T}_{\mathrm{en}} = \mathcal{T}\hat{\tau}_z = i\hat{\tau}_x\hat{\sigma}_y\mathcal{K}$ with $\mathcal{T}_{\mathrm{en}}^2 = -1$ ($\mathcal{K}$ is the complex conjugation and $\hat{\tau}_{x,y,z}$ is a set of Pauli matrices).

Finally, we discuss the derivation and limits of validity of the Dirac equation. Here we provide a general discussion. For a more concrete discussion of specific symmetry-based schemes, see Sec. IV.C. The "valley" pseudospin $\hat{\tau}_z$ is defined starting with a geometry supporting a pair of symmetry-protected Dirac cones. Each pseudospin direction ($\tau_z = 1$ or -1) identifies a pair of bands that are degenerate at the tip of a cone (at $\mathbf{k} = \mathbf{k}_0$ or $-\mathbf{k}_0$) but are coupled by a symmetry-breaking gap-opening perturbation of the initial geometry, with coupling constant m. Equation (3) is derived by applying perturbation theory for quasidegenerate levels using the quasimomentum variation $\mathbf{p} = \mathbf{k} \pm \mathbf{k}_0$ as a small parameter (Semenoff, 1984; Mousavi, Khanikaev, and Wang, 2015; Wu and Hu, 2015; Brendel *et al.*, 2017), an approach known as $\mathbf{k}\cdot\mathbf{p}$ perturbation theory (Kittel, 2004; Marconcini and Macucci, 2011). We note that the Dirac equation is reliable if the Fourier transform $\tilde{\mathbf{\Psi}}(\mathbf{p})$ of the envelope function $\mathbf{\Psi}(\mathbf{x})$ is localized in the small region $|\mathbf{p}| \ll 1/a$. In this regime, the coupling between opposing pseudospins, which might lead to gapped edge bands and backscattering, is suppressed because it is mediated by the tails of $\tilde{\mathbf{\Psi}}(\mathbf{p})$ (Shah, Marquardt, and Peano, 2021). This reasoning also applies to the special case $\mathbf{k}_0 = 0$ for which the two counterpropagating edge states are localized in the same quasimomentum region but remain uncoupled in this region. In a closed-domain geometry, this mechanism allows topological waves to turn sharp corners with negligible backscattering; cf. Fig. 4(a). The condition $|\mathbf{p}| \ll 1/a$ sets a limit on both the longitudinal quasimomentum p_x and the transverse localization length ξ of the edge states. For sharp domain walls we have $\xi = v/m_{\mathrm{bk}}$ [cf. Eq. (4)]; therefore, $\xi \gg a$ imposes a limit on the mass parameter $m_{\mathrm{bk}} \ll v/a$, and thus on the bandwidth available for topological transport [cf. Fig. 4(c)]. This trade-off between backscattering suppression and bandwidth is eliminated for smooth domain walls (Shah, Marquardt, and Peano, 2021). Ultimately the bandwidth is limited because of the restriction on the longitudinal momentum $|p_x| \ll 1/a$. For $|m_{\mathrm{bk}}| \gtrsim v/a$, the Dirac equation is not valid across the entire bulk band gap because $|p_x| \gtrsim 1/a$ for $|\omega| \approx |m_{\mathrm{bk}}|$, at the edge of the bulk band gap. This typically leads to edge states that do not connect the upper and lower bulk bands; see Ren *et al.* (2022).

III. OVERVIEW: TOPOLOGICAL PHONON TRANSPORT

After having understood the general fundamental mechanisms behind topologically protected edge states, we now focus on mechanical vibrations. Adopting the usual terminology in the field, we often refer here to topologically protected phonon transport, even though all of the systems studied experimentally thus far are firmly in the classical regime, where many phonons are involved in the high-amplitude classical vibrational states. As long as one stays in the linear regime, the mathematics remains the same regardless of the amplitude and regardless of whether individual phonons can be excited and resolved.

Since the design of geometrical structures is key in this field, we decided to show a pictorial overview of some of the most relevant theoretical and experimental works from the field, in chronological order, in Figs. 5 and 6. Many of these works are described in Sec. IV.

A. Different classification criteria

It is useful to systematically classify these works according to several criteria. We adopt the following categories, which are used to label works in the timeline of Figs. 5 and 6. Beyond distinguishing experimental implementations from theoretical proposals, we show the typical length scales of the system. Since most possible future applications of interest will most likely be on a micrometer- or nanometer-scale chip, this is a crucial key characteristic. While theoretical proposals may not commit themselves to a certain length scale, they sometimes rely on a macroscopic setting or, alternatively, take care to present a design that would work on the nanoscale, which we try to indicate.

Furthermore, we can separate the different works based on the type of topological protection. We distinguish between systems that break time-reversal symmetry (and thus result in a Chern insulator) and setups that do not break the time-reversal symmetry.

Moreover, most works can also be classified according to one of the following three categories: discrete systems, acoustic-wave systems, or elastic-wave systems. The first category corresponds to edge states that are formed by vibrational excitations of discrete lattice sites, i.e., coupled modes in a lattice. Exemplary systems are coupled pendula and theoretical works that take tight-binding models as their starting point. In contrast, both acoustic- and elastic-wave systems start with a continuum description, although sometimes this might eventually be transformed into an effective coupled-mode theory. Acoustic-wave systems feature topological modes that appear in the continuous fields of the pressure distribution within fluids. The airflow in an array of solid steel rods or water waves in a pipe of changing diameters are systems of that category. Finally, systems with topological edge modes appearing in the continuous deformation field of solid materials, for example, suitably patterned slabs of silicon, are referred to as elastic-wave models. The distinction according to these three categories is not always clear cut, but we find it helpful nonetheless.

Overall the topological systems of interest in this Colloquium cover a broad range of carrier frequencies and unit-cell length scales, from the infrasonic to the hypersonic regime and from the micrometer to the meter scale; see the scatterplot in Fig. 7.

B. Evolution of research in this field: A chronological overview

In this section, we give an overview of the most salient early works in chronological order to provide some general context for the following sections, which aim to be comprehensive. The first work to point out that topologically protected transport of phonons is a possibility stems from the field of biophysics. In their pioneering early paper, Prodan and Prodan (2009) conjectured that under certain assumptions vibrational edge states may form at the ends of long macromolecules that are part of the cell skeleton, the so-called microtubules, provided that magnetic elements give rise to time-reversal symmetry breaking. This hypothesis remains to be tested.

Moving to the domain of deliberately engineered topological phonon transport, the first idea for how this might be realized was introduced in 2014. The approach discussed there (Peano *et al.*, 2015) employed the optomechanical coupling between light and mechanical modes to generate time-reversal symmetry breaking and a phononic Chern insulator. It also was the first work to describe a potential nanoscale implementation based on phononic crystals.

A few months later, it was pointed out that topological transport can also be designed in macroscale engineered systems of fluids, where time-reversal symmetry can be broken by circulating flows, which results in a Chern insulator for the acoustic modes propagating inside the fluid (Yang *et al.*, 2015). This was followed by further analyses of the circulating-flow scenario in different settings (Khanikaev *et al.*, 2015; Ni *et al.*, 2015). Fleury, Khanikaev, and Alù (2016) proposed implementing a Chern insulator in an array of coupled acoustic resonators by modulating their resonant frequencies via piezoelectric actuators.

At around the same time, many implementations of Chern insulators were proposed for discrete systems. Wang, Lu, and Bertoldi (2015) predicted chiral edge states in an array of gyroscopes coupled with springs. Alternatively, the Coriolis force was suggested to break the time-reversal symmetry in a lattice of mass coupled with springs (Kariyado and Hatsugai, 2015; Wang, Luan, and Zhang, 2015).

Realizing mechanical topological phases requires a high degree of control in the engineering of mechanical structures. Not surprisingly, therefore, the earliest successful experimental implementations of topological mechanical systems were established in the realm of macroscopic centimeter-scale systems, starting in 2015 with 2D arrays of coupled pendula (Süsstrunk and Huber, 2015) with time-reversal symmetry intact (modeling a topological insulator), and of coupled gyroscopes (Nash *et al.*, 2015) with time-reversal symmetry broken. These systems provided direct and convenient experimental access and attracted considerable attention to the possibilities of engineered topological transport in mechanical systems, paving the way for subsequent rapid developments.

Subsequent experimental works expanded into the domains of acoustic waves directed by engineered scatterers (He, Ni *et al.*, 2016; Lu *et al.*, 2017), and shortly thereafter elastic vibrations in metal plates patterned with holes (Vila, Pal, and Ruzzene, 2017; Miniaci *et al.*, 2018; Yu *et al.*, 2018). More recently Chern insulator phases have been realized for acoustic waves (Ding *et al.*, 2019) in the presence of the circulation of a setup similar to the aforementioned original proposal of Yang *et al.* (2015), and for elastic waves in an array of piezoelectric membranes (Darabi *et al.*, 2020.

In parallel developments, theoretical investigations continued to explore the potential for nanoscale and microscale topological vibrational materials, as previously discussed. The first theoretical work to present a design in this domain for time-reversal-preserved topological transport (Mousavi, Khanikaev, and Wang, 2015) relied on a freestanding patterned mechanical metamaterial with suitable symmetries.

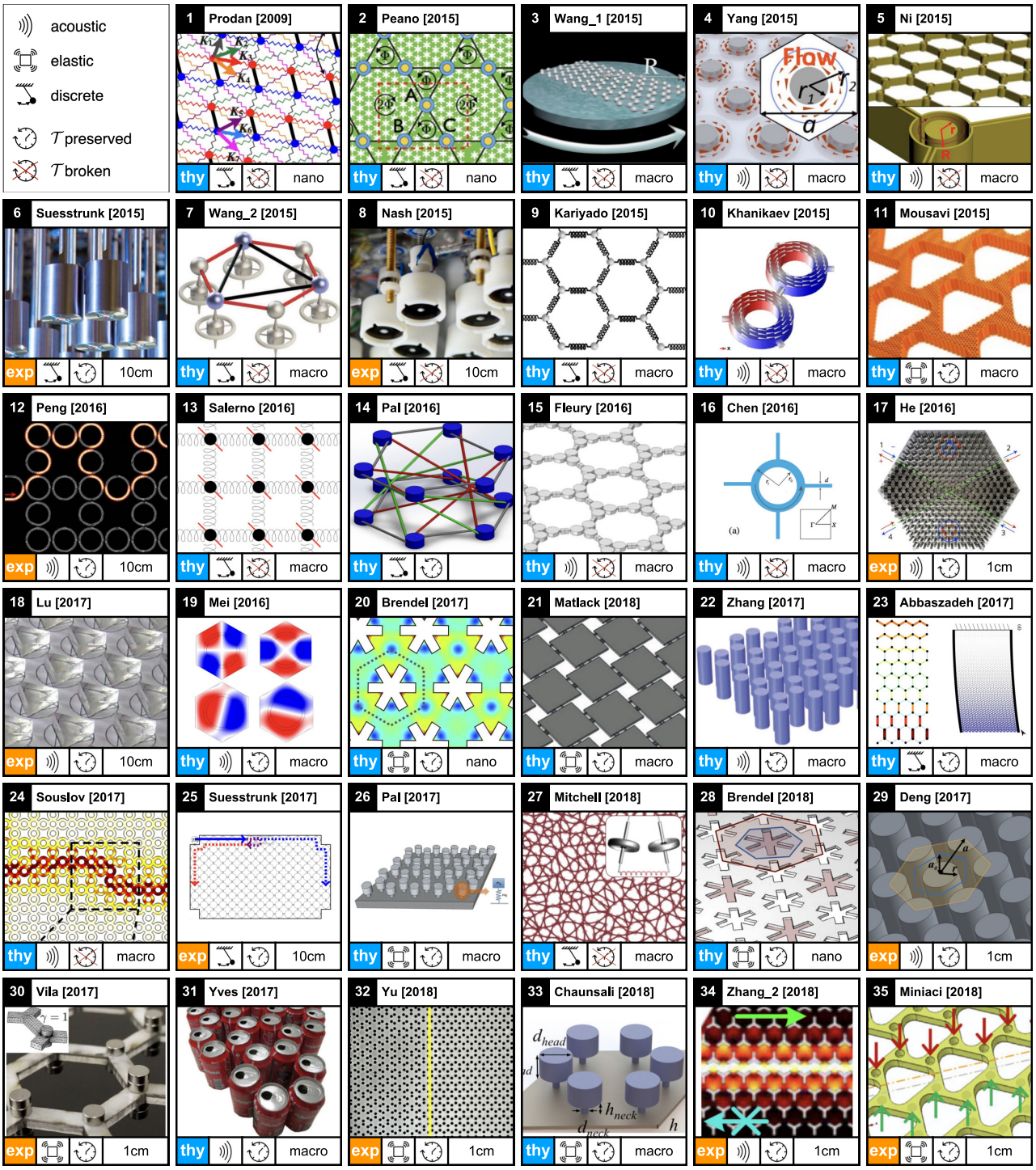

FIG. 5. Graphical timeline of works on topological transport in vibrational systems. We depict both theoretical proposals and experimental works. Each panel is labeled with the name of the first author. The icons indicate whether time-reversal symmetry is broken and whether the model employed in the work is based mainly on the coupling of discrete localized modes (pendulum symbol), the acoustics in gases or liquids (acoustic wave), or the elastic vibrations in solids (vibrating plate). The length scale is shown for experimental implementations. Whenever theoretical works propose concrete designs that can work at the nanoscale, this is indicated; likewise, we indicate when concepts by their nature are geared toward macroscopic or mesoscopic scales. From top left to bottom right (ordered according to first appearance in e-print form or journal submission date): Prodan and Prodan, 2009, Peano *et al.*, 2015, Wang, Luan, and Zhang, 2015, Yang *et al.*, 2015, Ni *et al.*, 2015, Süsstrunk and Huber, 2015, Wang, Lu, and Bertoldi, 2015, Nash *et al.*, 2015, Kariyado and Hatsugai, 2015, (Khanikaev *et al.*, 2015, Mousavi, Khanikaev, and Wang, 2015, Peng *et al.*, 2016, Salerno *et al.*, 2016, Pal, Schaeffer, and Ruzzene, 2016, Fleury, Khanikaev, and Alù, 2016, Chen and Wu, 2016, He, Ni *et al.*, 2016, Lu *et al.*, 2017, Mei, Chen, and Wu, 2016, Brendel *et al.*, 2017, Matlack *et al.*, 2018, Zhang *et al.*, 2017, Abbaszadeh *et al.*, 2017, Souslov *et al.*, 2017, Süsstrunk, Zimmermann, and Huber, 2017, Pal and Ruzzene, 2017, Mitchell *et al.*, 2018, Brendel *et al.*, 2018, Deng *et al.*, 2017, Vila, Pal, and Ruzzene, 2017, Yves *et al.*, 2017, Yu *et al.*, 2018, Chaunsali, Chen, and Yang, 2018, Zhang, Tian, Cheng *et al.*, 2018, and Miniaci *et al.*, 2018.

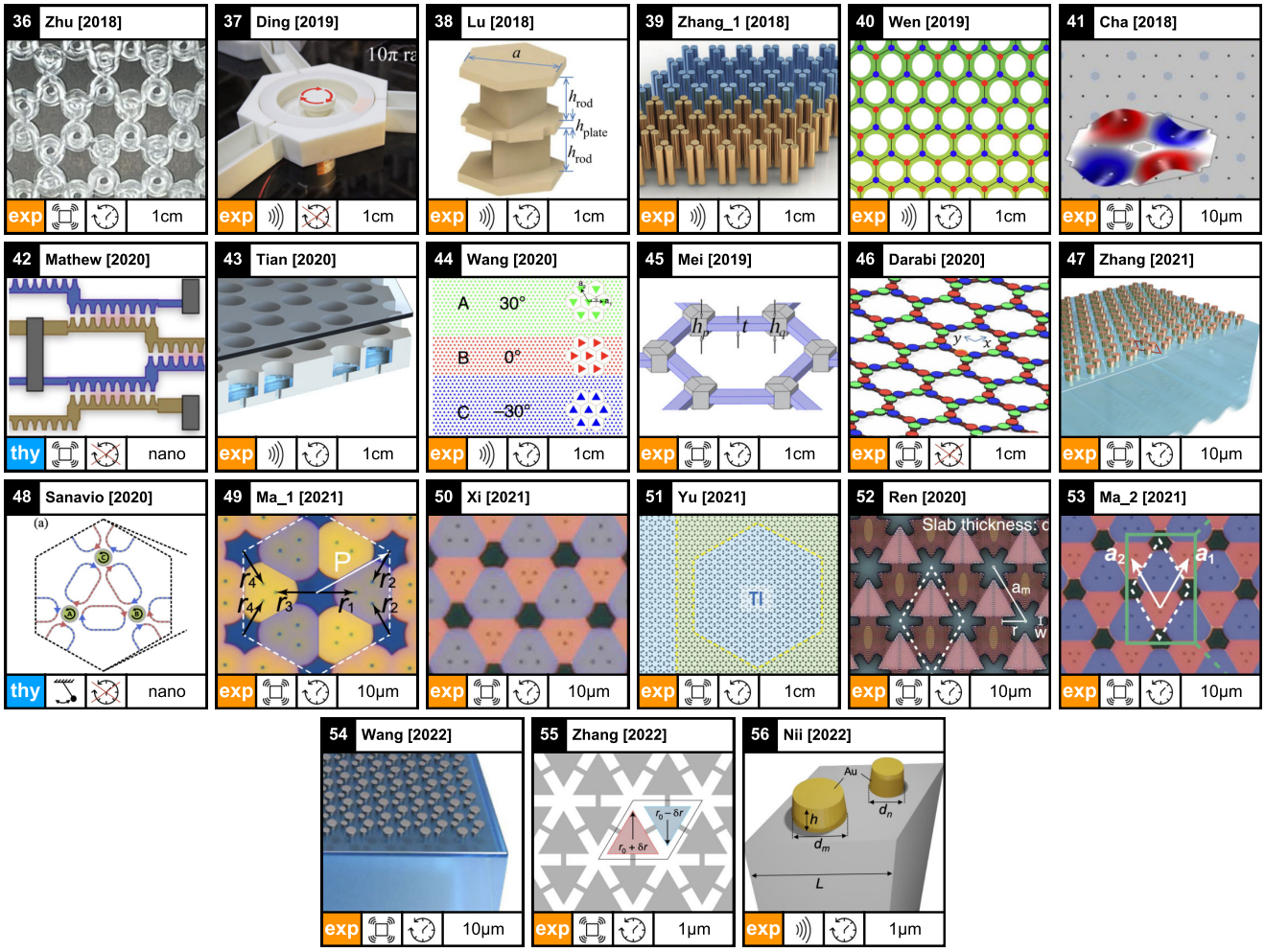

FIG. 6. Graphical timeline of works (continued). From top left to bottom right: Zhu, Liu, and Semperlotti, 2018, Ding *et al.*, 2019, Lu *et al.*, 2018, (Zhang, Tian, Wang *et al.*, 2018, Wen *et al.*, 2019, Cha, Kim, and Daraio, 2018, Mathew, del Pino, and Verhagen, 2020, Tian *et al.*, 2020, Wang *et al.*, 2020, Mei *et al.*, 2019, Darabi *et al.*, 2020, Zhang *et al.*, 2021, Sanavio, Peano, and Xuereb, 2020, Ma *et al.*, 2021, Xi *et al.*, 2021, (Yu *et al.*, 2021, Ren *et al.*, 2022, Ma, Xi, and Sun, 2021, Wang *et al.*, 2022, Zhang *et al.*, 2022, and Nii and Onose, 2023.

Other works in this direction used honeycomb (graphene-type) lattices, either producing pseudomagnetic fields via engineered distortions (Brendel *et al.*, 2017) or adopting enlarged unit cells (Brendel *et al.*, 2018).

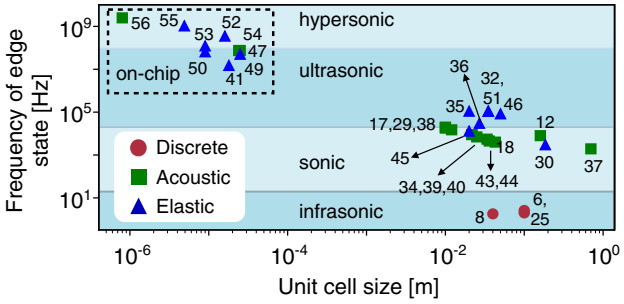

FIG. 7. Classification of different experimental works based on the frequency of the phononic edge channel and the size of the unit cell. The different categories of mechanical systems are discrete macroscopic systems, acoustic systems, and elastic systems. The numerical labels refer to the indices of the respective works in the timeline of Figs. 5 and 6 and show a trend toward on-chip small-fingerprint high-frequency devices.

Building on these proposals as well as recent advances in microfabrication techniques, the first on-chip nanoscale topological phonon transport was realized in 2018 (Cha, Kim, and Daraio, 2018) and followed by recent further promising experimental developments in this direction (Mathew, del Pino, and Verhagen, 2020; Ma *et al.*, 2021; Ma, Xi, and Sun, 2021; Xi *et al.*, 2021; Ren *et al.*, 2022; Zhang *et al.*, 2022). Beyond freestanding devices, topological waves also can be engineered on chip in the form of surface acoustic waves, as recently demonstrated in three pioneering experiments (Zhang *et al.*, 2021; Wang *et al.*, 2022; Nii and Onose, 2023). These efforts are part of an ongoing quest to reduce the footprint and increase phonon frequencies and bandwidths, as well as to explore more versatile actuation and detection schemes.

IV. APPROACHES FOR ENGINEERING TOPOLOGICAL TRANSPORT OF PHONONS

A. Electrons versus electromagnetic waves versus vibrations

The underlying mathematics of topological protection is equivalent for any kind of waves, be they electronic matter

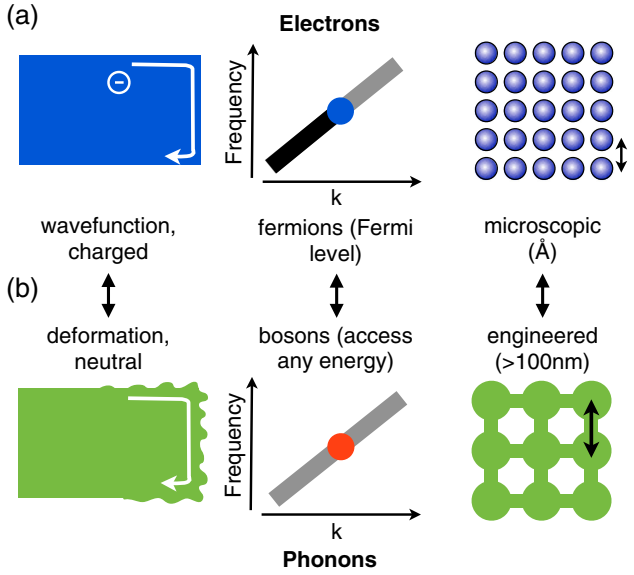

FIG. 8. Main differences between (a) electrons and (b) phonons from the perspective of topological transport. Left column: electronic transport can be affected by magnetic fields or spin-orbit coupling, while the transport of neutral phonons requires different approaches. Middle column: while electronic transport typically involves only states at the Fermi level, vibrations can be excited at any frequency in the band structure. Right column: electronic topological transport may exploit the microscopic crystal structure, while phononic transport is engineered on larger length scales (nanoscopic up to macroscopic).

waves, electromagnetic waves, or vibrational waves, as long as interactions can be neglected. Nevertheless, there are fundamental physical differences: distinguishing between fermionic and bosonic systems, but also differences with respect to other characteristics like the presence of a charge and the typical length and frequency scales that need to be manipulated in engineered structures. These differences lead to distinct, platform-specific approaches for implementing and exploiting topologically protected waveguides; cf. Fig. 8.

Electrons are charged and can therefore be manipulated with the help of electromagnetic fields. Breaking the time-reversal symmetry is straightforward using a static magnetic field, which produces the quantum Hall effect, a Chern insulator, with its characteristic robust protection. The fermionic nature of electrons implies that transport properties are affected only by the electronic matter waves near the Fermi energy, up to which all of the levels are occupied.

By contrast, electromagnetic waves and vibrational waves are neutral, so breaking the time-reversal symmetry needs to be engineered with some effort, such as via some form of time-dependent driving, as detailed in Sec. IV.B. Alternatively, one can rely on geometrical engineering to produce time-reversal-preserved systems that are the counterparts of the electronic topological insulators (which, in the electronic domain, arise from spin-orbit coupling). Both types of waves, electromagnetic and vibrational, are also bosons. There is no Fermi energy, and waves can be injected and probed at any frequency. One can view this as a unique advantage over electrons since it allows easy access to the full band structure and all edge states. At the same time, this also means that interactions (i.e., nonlinearities in the wave equation) can more easily scatter waves into other states, while these effects are suppressed for electrons due to the Pauli principle.

There are differences regarding scales that are important for engineering. Electronic wave functions live in materials with angstrom lattice periodicity, and "engineering" takes place via chemistry, apart from the comparatively rare cases where one relies on the design of superlattices. By comparison, both photonic and phononic wave functions are being engineered on a wide range of length scales, depending on the frequency, ranging from macroscopic centimeter-scale setups down to 100 nm. The methods employed encompass tools as diverse as 3D printing and lithography.

Thus far we have highlighted the similarities between sound waves and electromagnetic waves, contrasting them with electronic matter waves. However, in a number of aspects that are important for topological transport sound and light differ considerably. Differences include the possibility of engineering fluid flows for time-reversal-symmetry breaking of sound waves, the fact that vibrational waves are necessarily confined to the material and cannot radiate away energy into free space nearly as easily as electromagnetic waves, and their compact footprint (small wavelength) at a given frequency. We now turn to the core of this Colloquium: a detailed discussion of the different engineering approaches employed in the literature to implement topological transport in mechanical systems.

B. Broken time-reversal symmetry: Chern insulators

As mentioned, Chern insulators have been discovered by analyzing the dynamics of 2D electrons in an external magnetic field (Klitzing, Dorda, and Pepper, 1980; Thouless *et al.*, 1982). If a particle of charge q travels clockwise around a loop containing a magnetic flux Φ, then it will pick up a phase $q\Phi/\hbar$. Reversing the direction of the loop also reverses the sign of the phase acquired, indicating that the time-reversal symmetry has been broken. Since phonons do not have a charge, this mechanism is not directly available for vibrations. However, any physical mechanism that breaks time-reversal symmetry can potentially give rise to phases of this kind, and thus also the physics of charged particles in a magnetic field.

Taking advantage of this way of thinking, it is possible to build Chern insulators for phonons by engineering complex hopping amplitudes between the lattice sites such that the total phase picked up by a phonon around a closed loop is nonzero. We remark that these complex amplitudes are, in most cases, matrix elements of effective Hamiltonians defined in a rotating frame after a rotating-wave approximation.

Incidentally, there is no need to mimic a constant magnetic field in order to obtain edge channels. This was demonstrated by the Haldane model, which is the prototypical example of a tight-binding model with broken time-reversal symmetry but zero average magnetic field. In this model, charged excitations can hop on a honeycomb lattice via nearest-neighbor and next-nearest-neighbor transitions with probability amplitudes J_1 and $J_2 \exp(\pm i\phi)$, respectively. An excitation moving on a closed loop around a triangular plaquette picks up a

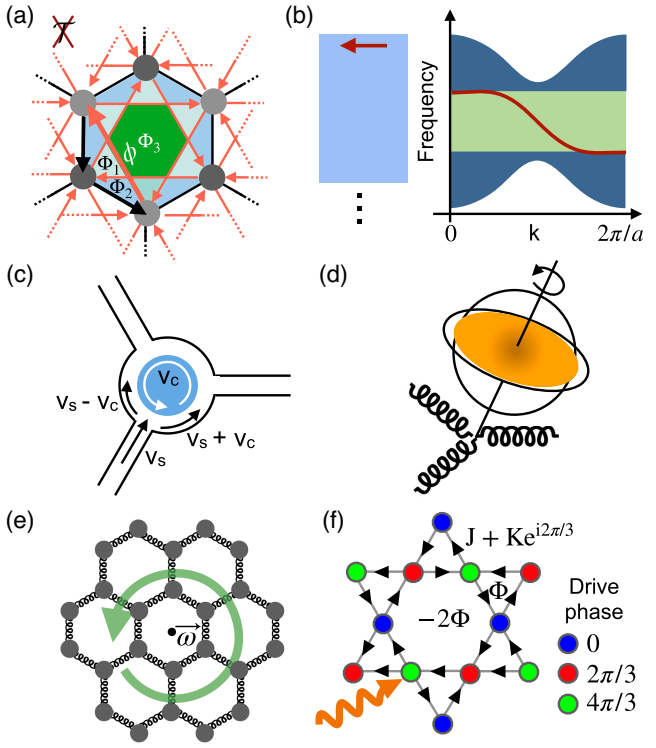

FIG. 9. Chern insulators. (a) Haldane model. Excitations hop on a honeycomb lattice between nearest-neighbor and next-nearest-neighbor sites. Regions pierced by the same magnetic flux Φ_1, Φ_2, or $\Phi_3 = -6(\Phi_1 + \Phi_2)$ are highlighted in the same color. All next-nearest-neighbor transitions in the direction indicated by the arrow have the probability amplitude $J_2 \exp(i\phi)$, with $\phi = 2\pi(\Phi_1 + 2\Phi_2)/\Phi_0$ and Φ_0 the magnetic-flux quantum. (b) Band structure (right sketch) of the semi-infinite translationally invariant strip configuration (left sketch; infinitely extended in the horizontal direction). The topological edge mode (red curve) connects subsequent bulk bands. (c)–(f) Different mechanisms to break the time-reversal symmetry in topologically protected phononic systems: (c) The rotating blue cylinder generates a fluid flow that results in a different sound speed along the two circulation directions of the acoustic waves, thus breaking time-reversal symmetry (Khanikaev *et al.*, 2015; Ni *et al.*, 2015; Yang *et al.*, 2015; Chen and Wu, 2016). (d) Precession of a spinning gyroscope, part of a lattice connected with springs (Nash *et al.*, 2015; Wang, Lu, and Bertoldi, 2015; Mitchell *et al.*, 2018). (e) Rotation of a lattice to create a Coriolis force acting on spring-coupled masses (Kariyado and Hatsugai, 2015; Wang, Luan, and Zhang, 2015). (f) Time-dependent modulation of lattice sites in a chiral fashion, such as using optomechanical interactions and suitable illumination or other mechanisms (Peano *et al.*, 2015; Fleury, Khanikaev, and Alù, 2016; Darabi *et al.*, 2020; Mathew, del Pino, and Verhagen, 2020).

nonreciprocal phase, for example, the phase ϕ following the thick arrows in Fig. 9(a). These nonreciprocal phases can be viewed as being induced by a staggered magnetic field as shown in Fig. 9(a). Haldane demonstrated that this configuration leads to topological bulk band gaps and the associated gapless edge states; cf. Fig. 9(b). Haldane further pointed out that an interaction breaking the inversion symmetry, in the form of different on-site energies on the two sublattices [the shades of gray in Fig. 9(a)], could induce a transition to a topologically trivial phase. Haldane's prototypical model highlights two key features of Chern insulators: (i) The breaking of time-reversal symmetry is the key precondition allowing bands with nontrivial Chern numbers. (ii) Time-reversal-symmetry-breaking perturbations favoring topological band gaps are in competition with inversion-breaking perturbations favoring trivial band gaps.

Although phonons are neutral excitations, an external magnetic field can still break the time-reversal symmetry for lattice vibrations. Analogously to the magneto-optical effect, a magnetic coupling can be mediated by charged particles in the hosting material. This mechanism leads to the phonon Hall effect (Strohm, Rikken, and Wyder, 2005) and in a suitable lattice geometry would also lead to a topological band structure supporting nontrivial Chern numbers. This idea was at the core of the first pioneering analysis of topological lattice vibrations (Prodan and Prodan, 2009; Zhang *et al.*, 2010; Qin, Zhou, and Shi, 2012). In the first theoretical analysis of phononic topologically protected edge states in any system, Prodan and Prodan (2009) presented the hypothesis that topological effects could play a role in the vibrational modes of microtubules, i.e., the self-assembled hollow protein tubes that are part of the cytoskeleton of living cells. They modeled the microtubule as a folded 2D lattice of dimers and speculated that the time-reversal symmetry may be broken by some magnetic properties of the surrounding medium. Shortly thereafter Zhang *et al.* (2010) and, subsequently, Qin, Zhou, and Shi (2012) showed that an external magnetic field would give rise to Chern insulator phonon bands for a simple bipartite ionic crystal and analyzed the footprint of the underlying band topology on the thermal Hall conductivity.

Given that the bandwidth of the topological excitations for crystal lattice vibrations is expected to be small, subsequent theoretical (Zhang and Niu, 2015; Nomura *et al.*, 2019) and experimental (Zhu *et al.*, 2018; Xu *et al.*, 2020) research focused on nontopological bulk transport. As predicted by Nomura *et al.* (2019) and later demonstrated by Xu *et al.* (2020), the combination of an external magnetic field and a lattice with broken inversion symmetry can give rise to the nonreciprocal bulk propagation of chiral lattice vibrations, which is known as the magnetochiral effect. Similar nonreciprocal bulk propagation has been predicted (Zhang and Niu, 2015) and experimentally demonstrated (Zhu *et al.*, 2018) in setups in which the time-reversal symmetry is broken by driving a chiral crystal with polarized light.

Moving on from examples of potentially naturally occurring topological transport of sound waves, we now turn to ideas for designing artificial structures. The first such idea (Peano *et al.*, 2015) proposed exploiting the coupling between light and sound to generate the required time-reversal symmetry breaking. The starting point would be a suitably engineered phononic crystal with micrometer-scale unit size, in this case consisting of a kagome pattern of coupled mechanical subunits. Using the principles of cavity optomechanics, the interaction between light and sound could be boosted by embedding photonic-crystal defect cavities, thereby creating an optomechanical array. When the entire structure is illuminated by a superposition of three laser beams, optical vortices are formed that impose their

nonvanishing orbital angular momentum on the sound waves via the optomechanical interaction. The resulting driving laser phases have a phase difference of $2\pi/3$ between neighboring sublattices; cf. Fig. 9(f). The combination of the choice of lattice and of the laser phases allows one to open band gaps between subsequent bands by breaking the time-reversal symmetry while maintaining the inversion symmetry. As discussed for the Haldane model in Sec. IV.B, this leads to a Chern insulator band structure, with topologically protected edge channels around the boundaries of the sample. The possibilities offered by this approach include *in situ* time-dependent switching of topological domains via the light. Depending on parameters, one can choose to have only a small admixture of photonic excitations or deliberately enter a regime of strong hybridization and topological transport of combined photon-phonon excitations. This proposal pointed the way toward nanomechanical topological phonon transport, and experiments in recent years are moving closer to eventually realizing such ideas, with Ren *et al.* (2022) having already shown 800 unit cells in an optomechanical array.

Other proposals based on optomechanical arrays were recently put forward (Mathew, del Pino, and Verhagen, 2020; Sanavio, Peano, and Xuereb, 2020). Sanavio, Peano, and Xuereb (2020) proposed an implementation based on optomechanical microtoroids. In their approach, the array is driven only from the perimeter, and neighboring microtoroids are coupled via the evanescent radiation without any direct mechanical coupling. If the optical modes are engineered to have a spin-orbit coupling (Hafezi *et al.*, 2013), the optomechanical interaction induces a nonreciprocal mechanical coupling between the breathing modes. The approach of Mathew, del Pino, and Verhagen (2020), with time-dependent modulation of the laser intensity generating coupling between mechanical modes of different frequencies, required less precise control of the optical modes and experimentally demonstrated a building block of the envisaged lattice. Similar schemes involving the parametric modulation of an array of mechanical oscillators with a periodic pattern of phase delays have also been proposed for arrays of pendula (Salerno *et al.*, 2016) and of acoustic cavities (Fleury, Khanikaev, and Alù, 2016). Both works also investigate the full time-dependent dynamics beyond the rotating-wave approximation, using the Floquet formalism. More recently the driving protocol and geometry of Fleury, Khanikaev, and Alù (2016) (involving oscillator trimers arranged on a honeycomb lattice) has been experimentally demonstrated for an array of piezoelectrically modulated elastic membranes (Darabi *et al.*, 2020), thereby representing the first experimental realization of a Chern insulator for elastic waves.

A number of schemes employing time-reversal symmetry breaking are based on acoustic-wave propagation in fluids. The unit-cell lengths for these systems are on the centimeter scale. The initial theoretical proposal by Yang *et al.* (2015), followed by Khanikaev *et al.* (2015) and Ni *et al.* (2015) and experimentally demonstrated by Ding *et al.* (2019), involved breaking the time-reversal symmetry by running a circulating airflow around cylinders. Owing to this external airflow, the acoustic-wave speed in the direction along the flow and opposite to it is different. In this way, the wave picks up a different propagation phase in the clockwise and the counterclockwise directions [see Fig. 9(c)], effectively leading to an acoustic Aharonov-Bohm effect. Chen and Wu (2016) used this scheme to propose a tunable topological phononic crystal. In a conceptually similar setting, Souslov *et al.* (2017) proposed and theoretically analyzed the topological density waves appearing in a liquid composed of self-propelled particles.

Chronologically the first experimental implementation of a Chern insulator for mechanical vibrations was presented in early 2015, for a macroscopic system: an array of coupled spinning motor-driven gyroscopes on a honeycomb lattice (Nash *et al.*, 2015). The precession of the gyroscopes around the suspension point breaks the time-reversal symmetry. To provide the coupling, a small magnet is placed in each gyroscope, leading to a magnetic repulsion between neighboring gyroscopes that can be modeled as a spring; see Fig. 9(d). This array of about 50 gyroscopes, with centimeter-scale unit size, was then imaged directly in real time, revealing the chiral propagation of a wave packet along the boundary of the array. In addition, in 2015 a similar gyroscope-based platform was independently proposed by Wang, Lu, and Bertoldi (2015). Subsequently, following up on their own previously discussed experimental work, Mitchell *et al.* (2018) studied Chern insulators both theoretically and experimentally in an amorphous lattice of gyroscopes while analyzing the interplay with strong disorder.

An alternative mechanism to implement a Chern insulator phase for discrete coupled mechanical systems is to take advantage of the Coriolis force by rotating a lattice of masses coupled with springs, as illustrated in Fig. 9(e). This approach was advocated by Kariyado and Hatsugai (2015) and Wang, Luan, and Zhang (2015).

In summary, Chern insulators for vibrations have been proposed, and in a few cases already experimentally implemented, based on a variety of mechanisms. These include time-reversal symmetry breaking via magnetic interactions, optomechanical interactions, time-dependent piezoelectric modulation, circulating airflows, gyroscopic motion, and Coriolis forces.

C. Preserved time-reversal symmetry

While time-reversal symmetry breaking gives rise to robust edge states, it can sometimes be easier if no such measures are required. This is especially true for nanoscale systems, where purely passive geometric designs are easiest to implement.

In Sec. II.C, we identified two complementary approaches to implement helical edge states in bosonic systems: (i) an effective spin-Hall Hamiltonian (block-diagonal across the BZ and supporting an engineered time-reversal symmetry $\mathcal{T}_{\mathrm{en}}$) (cf. Sec. II.C.1) and (ii) via effective Dirac Hamiltonians describing selected bands in a limited quasimomentum region (cf. Sec. II.C.2). Here we discuss their corresponding implementations in phononic systems starting with the first approach.

1. Implementing spin-Hall Hamiltonians

How can the classical dynamics of coupled mechanical harmonic oscillators, governed by Newton's laws $m\ddot{r}_i = -\mathcal{D}_{ij}r_j$ ($\hat{\mathcal{D}}$ is the dynamical matrix), imitate the dynamics

of the spin-Hall Hamiltonian (2)? This question was addressed by Süsstrunk and Huber (2015), who provided the first experimental realization of a two-dimensional mechanical phononic topological insulator (as opposed to a Chern insulator). They employed an array of centimeter-scale macroscopic pendula, each of which has only one motional degree of freedom, but coupled pairwise in a suitably designed way with several mechanical springs. In this way, they created an entire array imitating the required dynamical matrix $\mathcal{D}$; see Fig. 10(a).

More specifically Süsstrunk and Huber (2015) considered two copies of the Hofstadter model (Hofstadter, 1976) with opposing magnetic field and one-third of the magnetic-flux quantum per plaquette; cf. Fig. 10(a). The Hamiltonian $\hat{H}$ is complex valued and cannot be easily realized with coupled harmonic oscillators. Therefore, a local unitary transformation $\hat{U} = \hat{u} \otimes \mathbb{1}_{\text{lattice}}$ is performed $\hat{U}^\dagger \hat{H}\, \hat{U} = \hat{\mathcal{D}}$ such that the dynamical matrix $\hat{\mathcal{D}}$ becomes real valued and symmetric. More explicitly, at each lattice site the pseudospin states $(\psi_\uparrow, \psi_\downarrow)$ of the double-Hofstadter model are related to the vibrations x and y of two pendula [Fig. 10(b)] via the unitary operation

$$\begin{pmatrix} \psi_\uparrow \\ \psi_\downarrow \end{pmatrix} = \hat{u} \begin{pmatrix} x \\ y \end{pmatrix}, \qquad \hat{u} = \frac{1}{\sqrt{2}} \begin{pmatrix} 1 & -i \\ 1 & i \end{pmatrix}. \tag{7}$$

Thus, the two pseudospin eigenstates of $\hat{H}$ can be seen as certain relative motion patterns of the two pendula at each lattice site, which would correspond to left- and right-hand circular polarization in electromagnetism. The directed link between two neighboring unit cells is characterized by four effective spring constants, grouped in a 2×2 matrix K, as shown in Fig. 10(c). The required matrix is determined by the hopping amplitudes in the target model,

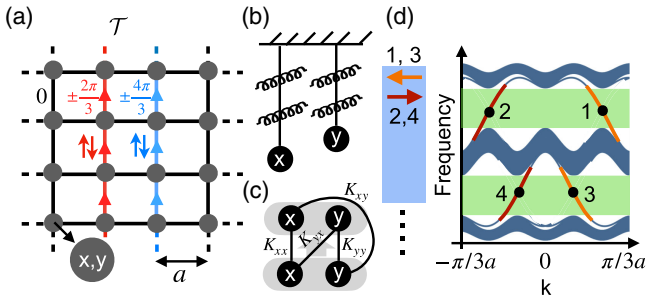

FIG. 10. Phononic spin-Hall Hamiltonians. (a) Two-copy version of the Hofstadter model. The phases $\pm\phi$ acquired by a pseudospin up and down hopping in the direction of the arrows for the three types of links (with varying shading) are indicated. Overall a pseudospin up (down) going around any plaquette acquires the Berry phase $2\pi/3$ ($-2\pi/3$). (b) The two modes x, y were realized by Süsstrunk and Huber (2015) as two one-dimensional pendula. (c) Definition of the matrix K. The unit cells are highlighted in gray. (d) Band structure (right sketch) of the semi-infinite strip configuration (left sketch) featuring topological edge states (red and orange arrows).

$$K(\phi) = J\hat{u}^\dagger \begin{pmatrix} e^{i\phi} & 0 \\ 0 & e^{-i\phi} \end{pmatrix} \hat{u} = J \begin{pmatrix} \cos\phi & \sin\phi \\ -\sin\phi & \cos\phi \end{pmatrix}. \tag{8}$$

In Eq. (8) ϕ ($-\phi$) is the phase acquired by a pseudospin up (down) excitation moving in the direction of the arrow between the unit cells; cf. Fig. 10(c). In the target model, $\phi = 0$, $2\pi/3$, and $4\pi/3$, respectively, for the black, red (dark gray), and blue (light gray) links in Fig. 10(a). Effective negative spring constants (required for $\phi \neq 0$) are engineered by coupling pendula via lever arms.

In a strip configuration, this particular system gives rise to two topological edge states in each of the two bulk band gaps, as illustrated in Fig. 10(d). The experiment of Süsstrunk and Huber (2015) demonstrated the existence of the edge states and tested their robustness against various boundary deformations. As a sequel to this work, they demonstrated the idea of switchable topological phonon channels in the same kind of platform (Süsstrunk, Zimmermann, and Huber, 2017).

The edge states demonstrated by Süsstrunk *et al.* are protected against any perturbation that preserves the engineered time-reversal symmetry $\mathcal{T}_{\text{en}} = \mathcal{U}\mathcal{T}$. Here $\mathcal{T}$ is the physical time-reversal symmetry and $\mathcal{U}$ is the local unitary symmetry $(x, y) \to (y, -x)$. We note that arbitrary disorder in the spring constants would preserve $\mathcal{T}$ but not $\mathcal{T}_{\text{en}}$, and thus can introduce backscattering. In other words, generic time-symmetric disorder coupling the two pseudospins plays the same role as magnetic disorder for an electronic topological insulator. This is generally true for any bosonic implementation of topological insulators. Although this seems like a great disadvantage, experiments and numerical simulations with moderate levels of geometrical disorder have shown the backscattering to be surprisingly small; see Süsstrunk and Huber (2015), Lu *et al.* (2017), and Brendel *et al.* (2018).

The implementation of spin-Hall Hamiltonians has also been proposed for phononic platforms other than arrays of pendula, including bilayer lattices of masses coupled via springs (Pal, Schaeffer, and Ruzzene, 2016) and elastic metamaterials (Matlack *et al.*, 2018) comprising perforated plates coupled by beams. In addition, Peng *et al.* (2016) proposed and experimentally demonstrated a topological insulator based on coupled-resonator acoustic waveguides. Their platform is the acoustic analog of the well-known topological photonics platform based on optical resonators coupled via coupler waveguides; see Hafezi *et al.* (2013). The relevant pseudospin is the chirality of the sound propagating clockwise or anticlockwise around a ring-shaped lattice resonator. It is conserved because the propagation direction does not change when the sound is transmitted between a lattice resonator and a coupling resonator. Peng *et al.* (2016) observed the topological phase transition predicted by Liang and Chong (2013) for symmetric couplers in the strong coupling regime. A similar platform was proposed by He, Li *et al.* (2016) for the spin-polarized transport of underwater sound. Beyond spin-Hall Hamiltonians, the connection between mass-spring models and single-particle quantum mechanical Hamiltonians was analyzed by Süsstrunk and Huber (2016), who developed a classification of the topological phases of such models based on the symmetry class and spatial dimension (in one, two, or three dimensions).

We now describe several schemes in which robust helical edge states are engineered via an effective Dirac Hamiltonian; see Sec. II.C.2. In these methods, the bulk normal modes need not be engineered across the BZ but only near some special high-symmetry points, based on robust symmetry-based designing principles. This family of approaches is particularly suitable for elastic vibrations and acoustic waves whose dynamics cannot be easily reduced to an effective tight-binding model.

2. Valley Hall

How can we most easily implement the Dirac Hamiltonian (3) in an engineered structure like a patterned slab or an array of scatterers? We start by observing that Dirac cones are ubiquitous for band structures in crystals in the wallpaper groups $p6$ (point group $\mathcal{C}_6$ formed by the sixfold rotations) or $p31m$ (point group $\mathcal{C}_{3v}$ with three mirror planes, each including a primitive lattice vector) when time-reversal symmetry $\mathcal{T}$ is respected. A prominent example is graphene. In this scenario, each Dirac cone stems from an essential degeneracy of two Bloch waves with opposing quasiangular momentum at the high-symmetry points $\mathbf{K}$ or $\mathbf{K}'$ of the Brillouin zone. The Dirac cones become gapped when the point group is reduced to $\mathcal{C}_3$; see Fig. 11(a). We thus arrive at Eq. (6), where $\tau_z = 1$ ($\tau_z = -1$) and $\mathbf{q} = \mathbf{k} - \mathbf{K}$ ($\mathbf{q} = \mathbf{k} - \mathbf{K}'$) in the valley around the high-symmetry point $\mathbf{K}$ ($\mathbf{K}'$). At a domain wall for the mass parameter, this leads to the appearance of a pair of counterpropagating edge channels, with each channel localized around a different valley; cf. Fig. 11(b). This is analogous to the quantum spin-Hall effect, with the two valleys playing the role of effective pseudospin directions, and it is known for this reason as the valley Hall effect.

The valley Hall effect was originally predicted for bilayer graphene (Martin, Blanter, and Morpurgo, 2008), where it was experimentally demonstrated by Ju *et al.* (2015). Subsequently, it has found fruitful application in engineered crystals. For these systems, it is straightforward to design a mass domain wall: any unit-cell geometry with weakly broken symmetry ($\mathcal{C}_2$ or $\mathcal{C}_v$) will have a mass parameter $m \equiv m_{\mathrm{bk}}$ (positive or negative). One can then obtain a suitable geometry with mass parameter $m = -m_{\mathrm{bk}}$ by simply applying the broken symmetry transformation to this unit cell; for example, the unit cell in the second domain is obtained by a 180° rotation of the unit cell in the first domain.

The first experimental implementation of acoustic topological edge states utilizing the valley Hall effect relied on acoustic waves propagating in a 2D lattice of triangular rodlike scatterers (Lu *et al.*, 2017); see Fig. 11(c). As the triangles are not aligned with the hexagonal lattice, a mismatch of mirror symmetries between the lattice and scatterers arises, breaking the $\mathcal{C}_{3v}$ symmetry, thereby producing the valley Hall effect and, eventually, the edge channels.

Various publications based on valley-polarized acoustic waves followed this initial work (Lu *et al.*, 2018; Wang *et al.*, 2018, 2020; Wen *et al.*, 2018; Xia *et al.*, 2018; Yang, Yang, and Zhang, 2018; Zhang, Tian, Cheng *et al.*, 2018; Zhang, Tian, Wang *et al.*, 2018; Han *et al.*, 2019; Shen *et al.*, 2019; Tian *et al.*, 2020; Fan *et al.*, 2022). Lu *et al.* (2018) proposed a bilayer design of scatterers for airwaves. Xia *et al.* (2018) demonstrated valley-polarized acoustic edge channels between a square lattice of scatterers, thereby going beyond the conventional triangular lattice employed in the valley Hall effect. The concept of topological acoustic valley transport has been leveraged to build acoustic antennas (Zhang, Tian, Wang *et al.*, 2018) and acoustic delay lines (Zhang, Tian, Cheng *et al.*, 2018); cf. Sec. VI. The acoustic antennas are used to out-couple airwaves from the lattice of rod-shaped scatterers to the surroundings in a desired direction, and to perform the reverse process of receiving sound only from a source in the desired direction. The delay line is used to control the time it takes for the energy to travel between two different points on a lattice. Zhang, Tian, Cheng *et al.* (2018) implemented acoustic delay lines using three-legged rod scatterers, where these rods can be rotated with computer-controlled motors to build reconfigurable topological edge states. An alternative recent implementation of tunable lattices, this one based on coupled acoustic cavities, was presented by Tian *et al.* (2020). With the goal of providing a more flexible interface to other acoustic devices, Wang *et al.* (2020) proposed and experimentally demonstrated a setup in which two topologically distinct domains were separated by a massless domain.

Approaches based on the valley Hall effect for elastic vibrations in macroscopic solids soon followed the

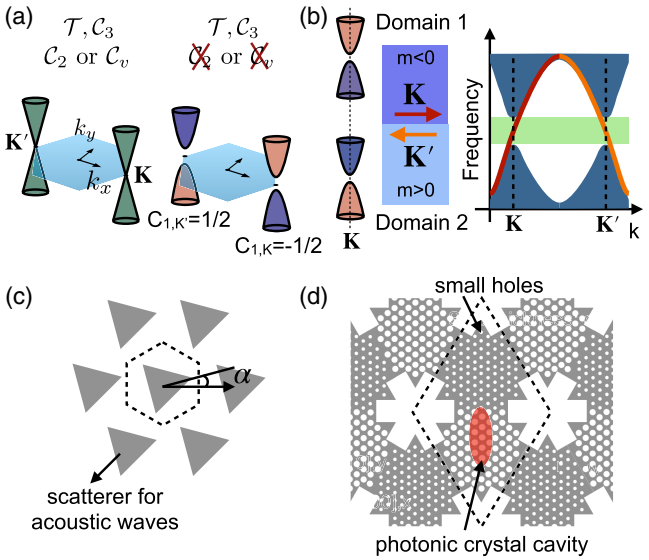

FIG. 11. Valley Hall effect. (a) Effect of different symmetries on the Dirac cones. The degeneracy splits on breaking the $\mathcal{C}_2$ or $\mathcal{C}_v$ symmetry of the original $\mathcal{C}_6$ or $\mathcal{C}_{3v}$ crystal. The shading of the resulting hyperbolic bands encodes the valley Chern number. (b) Left sketch: translationally invariant strip including two domains of opposite mass, with a helical edge channel arising at the domain interface (with the propagation direction depending on the valley index). Right sketch: the distinct valley Chern number C_{K} of the band for each domain. (c) Array of triangular scatterers for the acoustic waves discussed by Lu *et al.* (2017). The scatterers are rotated to break the mirror symmetry C_v, which opens a gap in the Dirac cones. (d) Implementation of the valley Hall effect in an optomechanical crystal (Ren *et al.*, 2022). The silicon slab consists of patterned holes of two different sizes, which are used to manipulate the Dirac cones. The vibrations are measured optically via the photonic-crystal cavity mode.

aforementioned first ideas for airflows (Huo *et al.*, 2017; Pal and Ruzzene, 2017; Vila, Pal, and Ruzzene, 2017). Pal and Ruzzene (2017) proposed an array of resonators arranged in a triangular lattice on an elastic plate. Vila, Pal, and Ruzzene (2017) implemented it experimentally by building a hexagonal elastic lattice out of an acrylic panel.

The first experimental demonstration of nanoscale topological phonon transport based on the valley Hall effect was recently presented. It utilizes an optomechanical array (Ren *et al.*, 2022) that is designed starting with a patterned Si slab phononic crystal with snowflake-shaped holes (Brendel *et al.*, 2017). The Dirac cones are gapped by breaking the $\mathcal{C}_v$ symmetry by engineering different properties of the A and B sublattice units. Furthermore, a photonic crystal is embedded inside the larger phononic unit cell; see Fig. 11(d). The purpose of producing an optical photonic-crystal defect cavity at each site of this array is to enhance the sensitivity of light-based detection of mechanical motion (by a factor of the finesse of the cavity). This allowed one, for the first time in any system, to measure thermal topological vibrations, of amplitudes around 10 fm, and to do so in a spatially resolved way by scanning along the domain wall. Valley-locked edge states have been demonstrated in other recent nanoscale experiments with surface acoustic waves (Zhang *et al.*, 2021) and in an array of suspended silicon nitride membranes (Ma, Xi, and Sun, 2021; Xi *et al.*, 2021) [similar to the setup used by Cha, Kim, and Daraio (2018) but with a different symmetry of the etching pattern; cf. Fig. 12(d)]. Zhang *et al.* (2022) reached the hypersonic regime for the first time using a piezoelectrically actuated aluminum nitride snowflake phononic crystal.

Next we highlight two important theoretical contributions to the general understanding of the valley Hall physics. Fan *et al.* (2022) drew an interesting connection between valley Hall edge states and the topological edge states of 3D Weyl semimetals. They focused on setups supporting a geometrical angle parameter α that controls the value of the mass parameter; cf. Fig. 11(c) for an example. Viewing this angle as the quasimomentum for a third synthetic dimension promotes the Dirac cones to 3D Weyl cones. In the presence of a straight boundary or domain wall, the valley edge states for varying values of the angle parameter α and longitudinal quasimomentum k are thus mapped onto the topological edge states of a Weyl semimetal. In addition, the synthetic quasimomenta (α and k) for the subset of valley edge states with eigenfrequency exactly in the middle of the bulk band gap form arcs in the α-k plane. Each arc connects the projections of a pair of artificial Weyl points onto this plane, analogous to Fermi arcs in Weyl semimetals (Wan *et al.*, 2011). Shah, Marquardt, and Peano (2021) analyzed the residual backscattering induced by large quasimomentum transfer, providing an interpretation of these transitions as tunneling processes in quasimomentum space; see Sec. V for further details.

3. Zone folding

The zone-folding scheme is an alternative symmetry-based approach to engineer an effective Dirac Hamiltonian with a tunable mass. As for the valley Hall effect, the Hamiltonian (6) is obtained by modifying an initial design

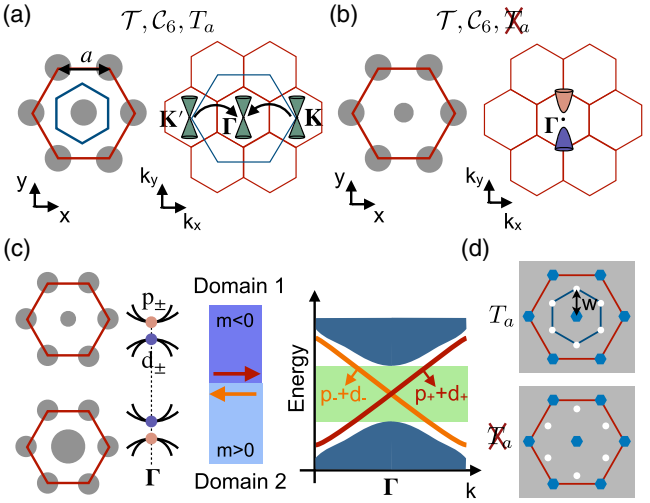

FIG. 12. Zone folding. (a) Left sketch: unit cell of an array of rod-shaped scatterers for acoustic waves used by Deng *et al.* (2017). Right sketch: description of the Dirac cone in k space for both the primitive (blue inner) and a larger (red outer) real-space unit cell, indicating the folding back to the Γ point. (b) Breaking the original discrete translational symmetry $\mathcal{T}_a$ by making the central rod smaller induces a gap in the Dirac cone. (c) Domain-wall configuration consisting of two domains with an inverted band arrangement. The radius of the central rod relative to that of its surroundings is varied in the two domains. The helical edge states appear in the bulk band gap of the strip band structure. (d) Schematic implementation of the zone-folding scheme for elastic waves on a patterned plate, as used in the experiment of Cha, Kim, and Daraio (2018). The distance w of the etched holes (white dots) from the blue center unetched region is varied to break the translational symmetry.

with $\mathcal{C}_6$ point-group symmetry that supports a pair of Dirac cones. In this scheme, the mass term is obtained by breaking the original translational symmetry without breaking the $\mathcal{C}_2$ symmetry. This generates a smaller Brillouin zone into which the original bands are folded back (hence the name). This scheme was originally proposed by Wu and Hu (2015) for photonic crystals.

The effective Hamiltonian for the previously described scenario is intimately connected to the valley Hall Hamiltonian. In both scenarios, one starts with the same assumptions leading to the effective Dirac equation [Eq. (6) with $m(\mathbf{x}) = 0$] before introducing the symmetry-breaking perturbation. We note that $\mathbf{q}$ is the quasimomentum of the enlarged unit cell. Thus, the band structure can be viewed as supporting a double Dirac cone (i.e., a doubly degenerate Dirac cone) centered at the Γ point of the reduced Brillouin zone; cf. Fig. 12(a). We further note that the Hamiltonian is invariant under any valley-admixing rotation of the pseudospin degree of freedom. In particular, one can combine the Bloch waves in the two valleys to obtain four $\mathcal{C}_6$-symmetric Bloch waves at the Γ point. It can be shown that under rotations they behave as $p_\pm$ and $d_\pm$ atomic orbitals (with quasiangular momenta ±1 and ±2, respectively). A perturbation that breaks the original translational symmetry T_a without breaking the $\mathcal{C}_6$ symmetry splits the degeneracy between the p and d Bloch waves, leading to a twofold

degenerate gapped cone band structure; cf. Fig. 12(b). As with the valley Hall effect, the underlying effective Hamiltonian has the form of Eq. (6). However, the rotated pseudospin τ_z now has a different interpretation: $\tau_z = 1$ ($\tau_z = -1$) if the carrier waves are p_+ or d_+ (p_- or d_-) Boch waves. This reflects the fact that, up to leading order in $\mathbf{k}$ for the $\mathbf{k}\cdot\mathbf{p}$ perturbation theory, only states that differ by one unit of quasiangular momentum are coupled. We note that $\tau_z\sigma_z = 1$ (-1) for the d (p) Bloch waves. In other words, the sign of the mass parameter m is set by the order of the p and d bands at the Γ points; see Fig. 12(c). Thus, a band inversion at the interface of two adjacent domains (here labeled types 1 and 2) gives rise to helical edge states; cf. Fig. 12(c).

The zone-folding idea was first transcribed from the photonic world to the phononic domain by Zhang *et al.* (2017), who theoretically proposed and analyzed the propagation of airborne sound in the presence of an array of cylindrical scatterers, in the same arrangement as the photonic-crystal holes in the first photonic proposal by Wu and Hu (2015). Shortly thereafter Yves *et al.* (2017) proposed using the same arrangement for an array of subwavelength Helmholtz resonators, in the form of soda cans, to engineer topological polaritonic waves. Chaunsali, Chen, and Yang (2018) employed the zone-folding idea to propose topological transport of flexural waves on a thin plate with resonators mounted on its top. The first experimental implementation of the zone-folding mechanism for mechanical topological transport (Deng *et al.*, 2017) employed an array of rodlike scatterers on a hexagonal lattice [see Fig. 12(a)], thereby shaping the acoustic vibrations of air between those rods.

Owing to its simplicity, zone folding was recognized as a promising approach for the nanoscale, with the first theory proposal based on elastic waves in a phononic crystal with snowflake-shaped patterned holes (Brendel *et al.*, 2018). Shortly thereafter Cha, Kim, and Daraio (2018) published the first experimental realization of an on-chip nanoscale topological metamaterial.

Their experiment is based on a zone-folding design, and their on-chip phononic crystal is made out of a piezoelectric material (SiN) to enable electrical signals to be transduced to mechanical motion. The schematic of the geometry is shown in Fig. 12(d), with a unit cell size of 18 μm and a frequency of around 15 MHz. They were able to detect in a space-time resolved way the propagation of wave packets along domain boundaries. This was achieved using an excitation electrode to inject flexural waves and a Michelson interferometer, which can be scanned, for optical detection. The zone-folding trick was also used for the first implementation of topological transport for surface acoustic waves (Zhang *et al.*, 2021).

Ma *et al.* (2021) proposed and experimentally demonstrated an interesting extension of the zone-folding trick. Their scheme features two different perturbations: the first breaks the translational symmetry $\mathcal{T}_a$ and the second breaks twofold rotational symmetry. The strengths of the two perturbations could be tuned independently by changing the appropriate geometrical parameters in the same platform used by Ma, Xi, and Sun (2021), allowing one to interpolate between the valley Hall Hamiltonians and the sixfold symmetric zone-folding ones while always keeping the same form of the effective Dirac Hamiltonian [Eq. (6)].

4. Accidental degeneracy of Dirac cones

The previously described zone-folding scheme provides a systematic engineering strategy to obtain double Dirac cones in a crystal: consider the band structure of the larger unit cell of a $\mathcal{C}_6$-symmetric crystal. In contrast, as the name itself suggests, the "accidental degeneracy" approach relies on fine-tuning. However, there is a logic behind the scheme, which is to take advantage of the fact that a $\mathcal{C}_6$-symmetric crystal automatically features the twofold degenerate symmetric states $p_\pm$ and $d_\pm$. If one can tune the parameters of the geometry so as to bring a pair of p and d states to the same frequency, then this would form a double Dirac cone at the Γ point; see the schematic bands in Fig. 13(b). Afterward one can follow the recipe that we described for the zone-folding scheme to create counterpropagating topological edge states out of a double Dirac cone.

The first experimental demonstration of phononic edge states produced via the accidental degeneracy mechanism was in the context of acoustic waves scattered by a lattice of steel rods (He, Ni *et al.*, 2016). By varying the ratio of the diameter of steel rods to the lattice periodicity across a threshold value, the order of a pair of p and d Bloch waves can be exchanged; cf. Figs. 13(a) and 13(b). Close to the Γ point and for ratios in the vicinity of the threshold value, the group of four bands is described by the Hamiltonian (6), allowing helical edge states to be engineered at a domain wall for the mass parameter. We note that essentially the same scheme was independently proposed by Mei, Chen, and Wu (2016). Going back to He, Ni *et al.* (2016), their setup featured a new way of arranging the two domains in a beam-splitter-like arrangement that has since also been useful in helical edge-state implementations to deduce to what extent the helical transport is spin polarized. The approach based on the accidental degeneracy of pairs of p and d Bloch waves has been also leveraged to implement topological elastic vibrations in a patterned plate; see Yu *et al.* (2018, 2021).

There is an alternative approach for obtaining degenerate Dirac cones accidentally that again involves not only fine-tuning but also use of the symmetries. As for the valley Hall effect, one starts with a geometry with a wallpaper group supporting symmetry-protected Dirac cones at the $\mathbf{K}$ and $\mathbf{K}'$ points. Typically planar geometries (such as phononic crystals and flexible plates) used for engineered 2D transport have an out-of-plane mirror symmetry M_z for reflection about the 2D plane. This prevents the mixing of modes that are symmetric and antisymmetric with respect to this symmetry. Therefore, if one can tune the geometry to bring the two Dirac cones corresponding to these two modes to have the same Dirac speed and degeneracy point, then they form a double Dirac cone at the $\mathbf{K}$ and $\mathbf{K}'$ points; see the schematic bands in Fig. 13(d). Subsequently the mirror symmetry is broken to produce a tunable mass term and to eventually create a domain wall between two topologically distinct domains. This leads to a pair of counterpropagating edge states at each Dirac point. The underlying Hamiltonian can be viewed as comprising two copies of Eq. (6).

This idea was presented early on by Mousavi, Khanikaev, and Wang (2015). In their design, they proposed plates patterned with holes arranged in a triangular lattice. The

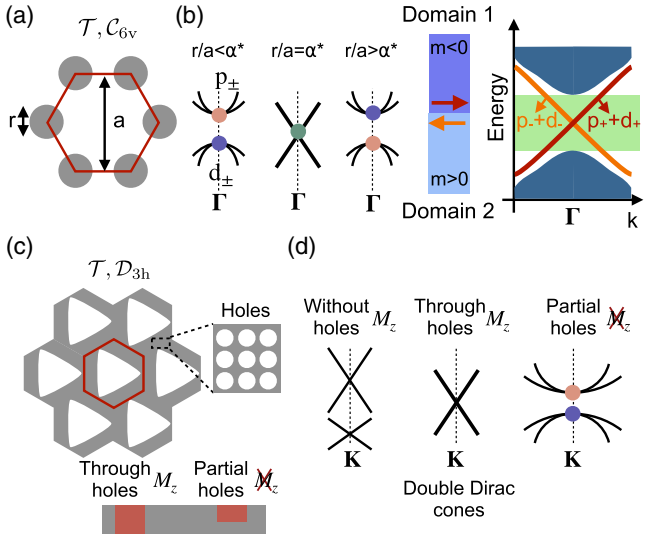

FIG. 13. Accidental degeneracy of Dirac cones. (a) Unit cell of an array of rods with $\mathcal{C}_{6v}$ symmetry acting as scatterers for acoustic waves (He, Ni *et al.*, 2016). (b) Left sketch: the ratio of the diameter to the periodicity is varied to observe the band inversion via a double Dirac cone at the Γ point. As in the zone-folding scheme, helical edge states appear in the bulk band gap. (c),(d) Metal plates patterned with holes of two sizes: large holes are used to obtain the Dirac cones at the **K** point for modes that are symmetric and antisymmetric about the *x*-*y* plane, as suggested by Mousavi, Khanikaev, and Wang (2015). The smaller holes [the inset in (c)] are used to engineer the dispersion for making the two cones identical. One can pattern partial holes to break the mirror symmetry M_z, and thereby gap the double Dirac cones (Miniaci *et al.*, 2018).

phononic crystal comprises two different feature sizes: the macrolattice is designed to create a pair of Dirac cones, whereas the smaller features on the microlattice are engineered to make the pairs of Dirac cones coincide not only in frequency but also in velocity. Inspired by this theoretical work, Miniaci *et al.* (2018) later experimentally demonstrated the accidental degeneracy of two Dirac cones in macroscopic patterned elastic plates. Another implementation based on an elastic rod lattice was demonstrated by Mei *et al.* (2019).

5. Pseudomagnetic fields

All schemes for engineering Dirac Hamiltonians presented thus far have in common that they make use of the mass term to generate topologically distinct domains, and thus helical edge states, at a smooth domain wall. An alternative to this approach is to use so-called pseudomagnetic fields. Pseudomagnetic fields are indistinguishable from magnetic fields if one is allowed to focus on a single pseudospin direction but have opposite signs for two pseudospins in opposite directions. This ensures that the time-reversal symmetry is preserved, in contrast to approaches in which the action of a magnetic field is mimicked across the Brillouin zone (as previously discussed for constructed Chern insulators). In graphene-based materials, pseudomagnetic fields are induced by position-dependent strain (Kane and Mele, 1997; Mañes, 2007). This gave rise to the idea (Guinea, Katsnelson, and Geim, 2010) to engineer constant pseudomagnetic fields via strain to observe quantum Hall physics that would otherwise require large magnetic fields, as demonstrated shortly thereafter (Levy *et al.*, 2010).

As with the other previously discussed Dirac-based approaches, pseudomagnetic fields can be understood by analyzing how the underlying Dirac Hamiltonian is modified after breaking a symmetry. In particular, we consider the same initial setup as in Sec. IV.C.2 (wallpaper group $p6$ or $p31m$ in the presence of the time-reversal symmetry $\mathcal{T}$), but now we analyze what happens after breaking the threefold rotational symmetry $\mathcal{C}_3$. In this case, the cones are not gapped (because the degeneracy is protected by the twofold rotational symmetry); rather, their tips are displaced away from the high-symmetry points **K** and **K**′. The location of the tip of the cone in relation to the high-symmetry **K**′ (**K**) point can be represented as a vector $\mathbf{A} = (A_x, A_y)$; see Fig. 14(a). Within a smooth-envelope approximation, the band structure in the vicinity of one of the valleys (say, the **K** point) is then described using the following 2D Dirac Hamiltonian:

$$\hat{H}_D(\mathbf{k}) = v[\mathbf{k} - \mathbf{K} - \mathbf{A}(\mathbf{x})] \cdot \hat{\boldsymbol{\sigma}}. \tag{9}$$

We observe that the quantity **A** is analogous to the magnetic vector potential for the case of a relativistic charged particle in a magnetic field. To use this effect to produce a pseudomagnetic field $\mathbf{B} = \nabla \times \mathbf{A}(\mathbf{x})$ for phonons, **A** must vary spatially, i.e., the location of the cone in momentum space needs to shift as one moves along in real space. This can be achieved by having a spatially varying deformation of the ideal phononic-crystal geometry; see Fig. 14(b). For a constant magnetic field in the z direction $\mathbf{B} = B_0\mathbf{e_z}$, a typical choice is to use the

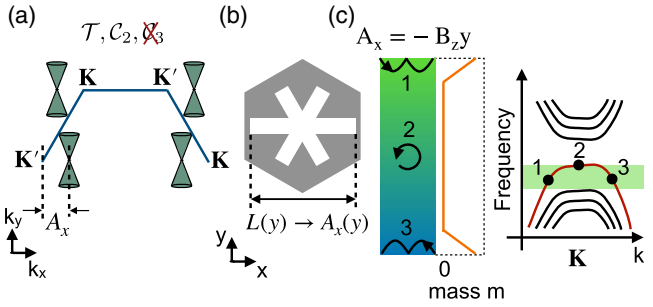

FIG. 14. Pseudomagnetic fields. (a) Upon breaking the $\mathcal{C}_3$ point-group symmetry, the Dirac cones shift in the Brillouin zone. The displacement from the valleys is given by $\mathbf{A} = (A_x, A_y)$ (here $A_y = 0$). (b) Scheme proposed by Brendel *et al.* (2017) to displace the Dirac cones in a phononic crystal. The horizontal arm length $L(y)$ of the snowflake-shaped hole is modified in a spatially dependent way, thereby inducing a spatial dependence $A_x(y)$. (c) Left sketch: translationally invariant strip with smooth boundaries. The gray scale encodes the vector potential A_x (for an out-of-plane constant magnetic field $\mathbf{B} = B_z\mathbf{e}_z$). Middle sketch: the position dependence of the mass parameter m defines the smooth boundaries. Right sketch: band structure in the vicinity of the **K** point. The bulk band gap between the $n = 0$ and $n = -1$ Landau levels is highlighted by shading. Away from the **K** point the Landau levels turn into gapless edge states. The semiclassical orbits for three modes are displayed in (c).

Landau gauge, i.e., to set $\mathbf{A} = -B_0 y \mathbf{e}_\mathbf{x}$, which implies a certain spatial pattern of deformation. The band structure then features Landau levels in the vicinity of the **K** and **K′** points. This also means that valley-polarized waves in the bulk of the material will experience a Lorentz force.

Pseudomagnetic fields were originally transferred from the electronic realm into the mechanical domain by Brendel *et al.* (2017), who considered a nanoscale phononic crystal implementation; see Fig. 14(b). The same concept was also analyzed for a tight-binding (mass-spring) mechanical model of strained graphene (Abbaszadeh *et al.*, 2017). More recently pseudomagnetic fields were implemented for acoustic waves by Wen *et al.* (2019). Apart from generating bulk pseudomagnetic fields, Brendel *et al.* (2017) also put forward the idea of using those fields to engineer gapless helical edge states analogous to their chiral counterparts in the presence of time-reversal-symmetry-breaking magnetic fields. As for other design schemes producing helical edge states based on the Dirac Hamiltonian, successfully achieving robust edge-state transport requires the coupling between different valleys to be suppressed by means of smooth domain walls or boundaries; cf. Figs. 14(c) and 14(d).

V. CHALLENGES FOR TOPOLOGICAL PHONON TRANSPORT

Various challenges will have to be addressed to fully realize the potential of topological phonon transport in actual applications. For instance, external modulation schemes are an important possibility in order to realize Chern insulators for phonons, but it is difficult to engineer them. As most future applications of topological phonon waveguides are envisaged for nanoscale devices, these engineering challenges will become even more formidable to solve. For example, it is not straightforward to achieve the required control of a platform to implement a spin-Hall Hamiltonian across the entire BZ. Even when this is possible, simple geometrical disorder can induce backscattering since Kramers degeneracy is enforced by an artificial symmetry ; cf. Fig. 15(a). As another example, the promising schemes of topological transport and phonon control in optomechanical arrays [starting with Peano *et al.* (2015)] in some cases rely on optical modes being tuned into resonance, which is still a challenge due to unavoidable fabrication disorder. More progress in this domain is needed, as it is for many other applications beyond topological transport.

Hence, approaches based on engineered Dirac cones are favored at the nanoscale (Cha, Kim, and Daraio, 2018; Ma *et al.*, 2021; Ma, Xi, and Sun, 2021; Xi *et al.*, 2021; Zhang *et al.*, 2021, 2022; Ren *et al.*, 2022; Wang *et al.*, 2022). Although for this case one can obtain Dirac cones by enforcing a suitable symmetry in the crystal, one still needs to perform additional engineering to get these cones spectrally isolated. That is, there should not be any other bands in the same frequency range; cf. Fig. 15(b). Moreover, the smooth-envelope approximation (and thus the suppression of backscattering) relies on the assumption that the edge states are well localized in quasimomentum. For this reason, tightly confined edge states are more prone to backscattering; cf. Fig. 15(c). For sharp domain walls this translates into a constraint on the bandwidth; see our discussion in Sec. III. In addition, the reflection strongly depends on the geometry and carrier frequency of the wave. For sharp turns connecting straight segments of the domain walls, it is well known that the reflection is strongly reduced for so-called zigzag segments oriented along the primitive lattice vector (of the smaller unit cell in zone-folding schemes); see Lu *et al.* (2017). Indeed, this type of domain wall is used in most experiments. The more detailed analysis given by Shah, Marquardt, and Peano (2021) advocated for smooth domain walls to eliminate the trade-off between backscattering and bandwidth. They further showed that in this scenario the backscattering takes place predominantly at certain locations that coincide with special values of the local angle of the domain-wall boundary; cf. Fig. 15(d). Future attempts at engineering topologically robust transport along edge channels in time-reversal-symmetric systems should take these observations into account.

Even when backscattering is negligible, there is one remaining challenge, namely, mechanical dissipation: phonons can simply get lost while traveling along the edge channel. This is a common problem for transport in any physical platform without particle number conservation, and it is shared by electromagnetic waves, in particular. Great effort has been expended over the past two decades to reduce

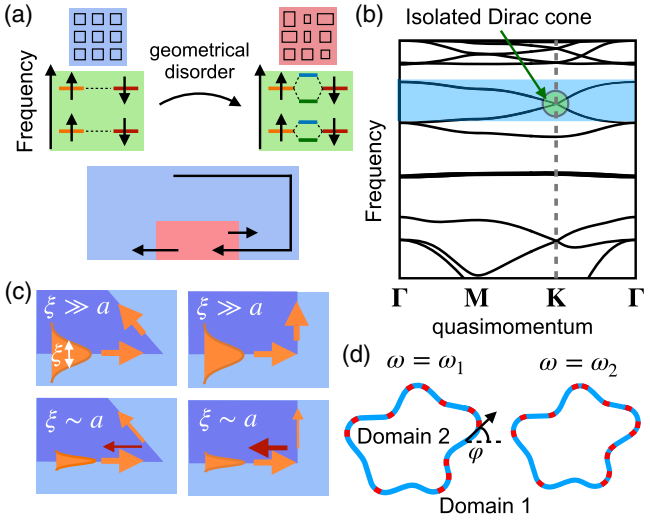

FIG. 15. Challenges for topological phonon transport. (a) Effects of geometrical disorder in time-reversal symmetric systems. Disorder coupling opposite pseudospin directions also breaks Kramers degeneracy (top sketch), and thus could induce backscattering (bottom bottom sketch). (b) Spectral isolation. Phonon band structure of an actual crystal featuring multiple Dirac cones at the **K** point in the Brillouin zone. The spectrally isolated Dirac cone is marked by a circle. (c),(d) Backscattering for edge states based on Dirac engineering. (c) Transport with tight vs weak transverse confinement. The reflection is guaranteed to be small only if the transverse localization length ξ exceeds the lattice spacing a. The reflection also depends on the domain-wall orientation (the thickness of the arrows represents the wave's intensity). (d) Backscattering for a smooth domain wall and two values of the carrier frequency ω. The reflection is enhanced at certain locations (the short red segments) that depend on both the frequency and the domain-wall orientation φ (relative to the microscopic lattice).

mechanical dissipation in nanomechanical systems (Cleland, 2003; Bachtold, Moser, and Dykman, 2022) since it represents an important issue for a number of applications ranging from sensing to quantum information processing. Strategies include the choice of suitable materials, care in preparing the surfaces, the design of geometries where clamping losses are minimized and strain is distributed in an optimized way, and high tensile stresses. Currently mechanical Q factors (the ratio of frequency and dissipation rate Ω/Γ) can reach 10^9 (Tsaturyan *et al.*, 2017) or more in gigahertz-frequency phononic-crystal platforms (MacCabe *et al.*, 2020), which may be suitable for conversion into topological waveguides.

VI. POTENTIAL APPLICATIONS AND FUTURE RESEARCH DIRECTIONS

Topological transport phenomena have been explored in a variety of physical platforms (such as electrons, atomic matter waves, electromagnetic waves, sound waves, and magnons). A strong motivating factor behind this research is the mathematical beauty of the underlying concepts and the fact that topological phenomena are generic and robust, and thus not dependent on small details of the implementation. However, even the first known incarnation of topological transport, for electrons in the quantum Hall effect, was quickly understood to be promising for applications. The precise quantization of the electrical conductance afforded by topological protection is now used to measure the Planck constant and define the kilogram. This history raises the question of which features of phononic topological transport may eventually become useful for real applications.

Such applications will want to employ the resilience of phononic topological waveguides against backscattering due to disorder and sharp turns; cf. Fig. 16(a). Additionally, in systems with time-reversal symmetry breaking, one can make use of the nonreciprocal nature of transport along the edge channels as well.

One such potential application is the delay line, which is used to add desired delays for energy to travel from a source to a detector. It can be implemented by simply elongating the length of the waveguide connecting the source and the detector. However, real applications for elastic-wave delay lines will typically rely on microscale or nanoscale systems, both to work in the required frequency band set by the application and to restrict the overall size of the device. To maximize the ratio of the waveguide length to the required footprint, one imposes several turns of the waveguide in a meandering structure; cf. Fig. 16(b). In this setting, topological phononic waveguides can then be employed to have sound travel through relatively sharp turns without any backscattering. This was previously explicitly suggested as an application for the topological transport of electromagnetic waves (Hafezi *et al.*, 2011) and then translated to sound waves (Zhang, Tian, Cheng *et al.*, 2018).

Another possible application is the so-called superdirectional acoustic topological antenna. The purpose of this device is to transmit sound in a desired narrowly focused direction, and likewise to receive sound only from a source in the desired direction; cf. Fig. 16(c). This has been demonstrated based on valley Hall waveguides for sound waves in air (Zhang, Tian,

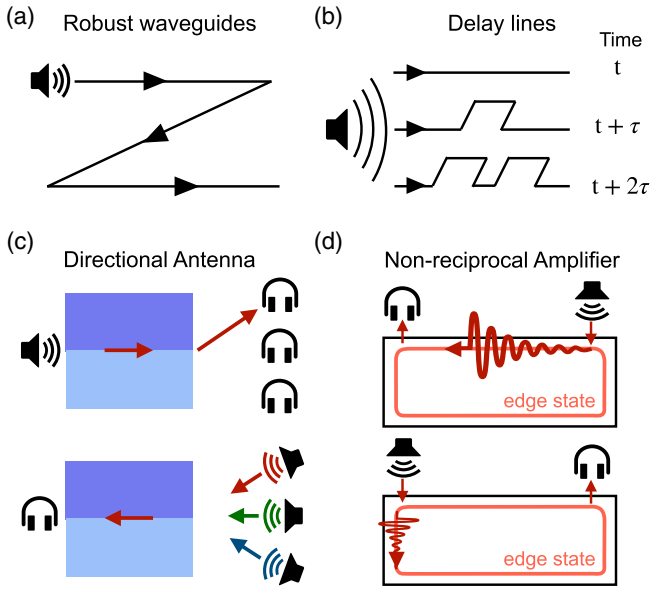

FIG. 16. Applications of topological waveguides. (a) The advantage of topological waveguides is that the transport is robust against sharp turns, permitting compact devices and some insensitivity to fabrication imperfections. (b) Topological delay lines constructed by elongating the path length with multiple loops between source and detector. (c) Topological directional antenna in a time-reversal preserved topological waveguide. The path between the source and the detector through the waveguide is indicated by the arrow. (d) Nonreciprocal amplifier. The signal is amplified when it travels from the source to the detector, but any noise going the other way will be deamplified, thus protecting the source.

Wang *et al.*, 2018). Provided that the interface at the edge of the device is properly designed, the valley-polarized character of sound transmitted along the waveguide guarantees that there is no undesired backscattering, in contrast to a standard waveguide. The directionality is controlled by the geometry, especially the lateral extent of the edge-state wave function.

Another promising potential application for unidirectional transport along topological edge channels is the nonreciprocal amplifier (Peano *et al.*, 2016). Such an on-chip device amplifies the signal coming from a source and injects the resulting amplified wave into a more conventional second-stage amplifier. The goal is to isolate the source (for example, containing a fragile quantum device) from any noise that may be injected back from the second-stage amplifier, which can be a serious technological concern. This goal can be realized by employing the unidirectional edge channels of a Chern insulator, with extra nonlinearities in the wave equation ensuring that external driving can provide an energy pump and amplification; cf. Fig. 16(d). Shortly after the proposal by Peano *et al.* (2016), a related version of this kind of physics was realized for photonic systems in the form of the topological insulator laser (Bandres *et al.*, 2018; Harari *et al.*, 2018), with pumped edge states exhibiting lasing. More generally, tuning dissipation and amplification (such as via optomechanical interactions and/or geometrical engineering) leads to the domain of non-Hermitian topology (Xu *et al.*, 2016; Bergholtz, Budich, and Kunst, 2021; del Pino, Slim,

and Verhagen, 2022), which likely will also become more prominent in the future for topological phononics.

Being able to control and reconfigure topological edge channels and rearrange their connectivity can greatly improve their usefulness. In photonic systems, some early proposals in this direction involved the macroscopic tunability of the platform (Cheng *et al.*, 2016; Zhao *et al.*, 2019). In vibrational topological systems, several ideas have been explored as well (Zhang, Tian, Cheng *et al.*, 2018; Darabi *et al.*, 2020; Tian *et al.*, 2020). Specifically, for nanoscale phonons an interesting possibility offered by optomechanics uses the optical spring effect to locally tune vibrational modes in and out of resonance, thereby enabling and blocking transport (Aspelmeyer, Kippenberg, and Marquardt, 2014). In this way, light could switch topologically robust phononic edge channels in real time.

Such reconfigurable networks of phononic edge channels could be used to connect on-chip quantum devices like spins, quantum dots, and superconducting qubits; see Habraken *et al.* (2012). They could also serve to study thermal and quantum transport of phonons in a new and unconventional but well-controlled regime (Barzanjeh, Aquilina, and Xuereb, 2018).

Thus far we have almost exclusively discussed purely linear dynamics, i.e., the propagation of noninteracting phonons (with the exception of the aforementioned amplifier physics, which relies on some nonlinearity for its implementation, but where the equations are nevertheless linear). A rich set of new phenomena become available when nonlinearities start to play a role. Owing to the typical strength of such nonlinearities in nanomechanical systems, it will be exceedingly difficult to observe them on the single-phonon level (unless nonlinearities are drastically increased by coupling to nonlinear quantum devices). However, even the classical dynamics of nonlinear waves in edge channels of topologically nontrivial systems is an interesting subject of study that has barely been explored. Most existing demonstrations and analysis to date have been based on photonic systems (Lumer *et al.*, 2013; Ablowitz, Curtis, and Ma, 2014; Leykam and Chong, 2016; Mukherjee and Rechtsman, 2020; Mittal *et al.*, 2021) [as reviewed by Smirnova *et al.* (2020)]. Nevertheless, the first ideas started to appear for implementing nonlinear topological phononics (Pal *et al.*, 2018; Chaunsali and Theocharis, 2019; Darabi and Leamy, 2019; Chaunsali *et al.*, 2021), where the nonlinearity affects the waves propagating along the edge channels and can even be responsible for producing such edge channels.

Enabling all of these applications requires inventive new designs, and the variety of approaches discussed in this Colloquium provide examples of that. Recently it was realized that deep learning methods can help with analyzing, predicting, and ultimately designing and optimizing topological band structures and topological transport. For example, Pilozzi *et al.* (2018) trained a neural network to predict topological band structures, taking as input a few parameters for simple tight-binding models. Going a step further, Peano, Sapper, and Marquardt (2021) showed that a neural network learned to predict topological band structures for arbitrary geometries of a crystal's unit cell provided as an image. The network was trained to output an approximate tight-binding model, taking into account existing symmetries of the problem, and it was used to optimize geometrical designs (made possible by the fact that neural networks are differentiable function approximators). Future studies in this direction will likely be of great help in engineering better platforms.

Regarding experiments, in our view the most important overall trend in topological phononics is the emergence of first nanophononic realizations of topological transport (Cha, Kim, and Daraio, 2018; Ma *et al.*, 2021; Ma, Xi, and Sun, 2021; Xi *et al.*, 2021; Zhang *et al.*, 2021, 2022; Ren *et al.*, 2022; Wang *et al.*, 2022; Nii and Onose, 2023). These are crucial, as they will pave the way toward truly useful devices. Such efforts are tied into the overall developments in the fertile areas of nanomechanics (Cleland, 2003; Bachtold, Moser, and Dykman, 2022) and optomechanics (Aspelmeyer, Kippenberg, and Marquardt, 2014), with ever greater control and ever better mechanical quality factors encompassing phononic crystals, the use of nanomechanics for sensing, and coupling to quantum devices.

VII. CONCLUSION

In this Colloquium, we have covered the recent developments of a wide range of ideas for engineering topologically protected transport of vibrations in the solid state and of sound waves in fluids. This field of topological phonon transport initially evolved out of a desire to explore and access, in vibrational and acoustic systems, the same conceptually interesting phenomena that had already been established for electrons and that had begun to be analyzed for electromagnetic waves and cold atoms as well. A fruitful combination of theory and experiment has since driven this field forward. Investigations on the experimental side started at the macroscale. At the same time, theoretical works were already exploring possibilities for future nanoscale platforms, where most of the promising applications for topologically protected transport of vibrations reside.

As devices are miniaturizing and becoming increasingly densely packed with time, the robustness of topological waveguides will help one to route the vibrations along desired paths without any scattering losses. The nonreciprocity in situations with engineered time-reversal symmetry breaking can be exploited for isolation, for example, in nonreciprocal amplification. Experimental efforts in the field of nanoscale topological phonon transport are currently in only their beginning stages, and the investigation of quantum phenomena is likewise an outstanding challenge.

To add to these promises, such devices can turn into hybrid platforms by incorporating coupling to microwaves, optical waves, or spin waves. This can enable novel possibilities like reconfigurable topological waveguides. All of these functionalities of topological vibrational waveguides make them a promising candidate to be used in future integrated phononic chips. Time will tell which of the many concepts and types of platforms covered in this Colloquium turn out to be the most suitable for future technological applications, and considerable further developments will be required toward this end.

ACKNOWLEDGMENTS

T. S. acknowledges support from the European Union Horizon 2020 research and innovation program under Marie Skłodowska-Curie Grant Agreement No. 722923 (OMT). F. M. acknowledges support from the European Union's Horizon 2020 research and innovation program under Grant No. 732894, Future and Emerging Technologies (FET)–Proactive Hybrid Optomechanical Technologies (HOT).

REFERENCES

Abbaszadeh, Hamed, Anton Souslov, Jayson Paulose, Henning Schomerus, and Vincenzo Vitelli, 2017, "Sonic Landau Levels and Synthetic Gauge Fields in Mechanical Metamaterials," Phys. Rev. Lett. **119**, 195502.

Ablowitz, Mark J., Christopher W. Curtis, and Yi-Ping Ma, 2014, "Linear and nonlinear traveling edge waves in optical honeycomb lattices," Phys. Rev. A **90**, 023813.

Aidelsburger, Monika, Sylvain Nascimbene, and Nathan Goldman, 2018, "Artificial gauge fields in materials and engineered systems," C. R. Phys. **19**, 394–432.

Asbóth, János K., László Oroszlány, and András Pályi, 2016, *A Short Course on Topological Insulators*, Lecture Notes in Physics Vol. 919 (Springer International Publishing, Cham, Switzerland).

Aspelmeyer, Markus, Tobias J. Kippenberg, and Florian Marquardt, 2014, "Cavity optomechanics," Rev. Mod. Phys. **86**, 1391–1452.

Bachtold, Adrian, Joel Moser, and M. I. Dykman, 2022, "Mesoscopic physics of nanomechanical systems," arXiv:2202.01819.

Bandres, Miguel A., Steffen Wittek, Gal Harari, Midya Parto, Jinhan Ren, Mordechai Segev, Demetrios N. Christodoulides, and Mercedeh Khajavikhan, 2018, "Topological insulator laser: Experiments," Science **359**, eaar4005.

Barzanjeh, Shabir, Matteo Aquilina, and André Xuereb, 2018, "Manipulating the Flow of Thermal Noise in Quantum Devices," Phys. Rev. Lett. **120**, 060601.

Barzanjeh, Shabir, André Xuereb, Simon Gröblacher, Mauro Paternostro, Cindy A. Regal, and Eva M. Weig, 2022, "Optomechanics for quantum technologies," Nat. Phys. **18**, 15–24.

Bergholtz, Emil J., Jan Carl Budich, and Flore K. Kunst, 2021, "Exceptional topology of non-Hermitian systems," Rev. Mod. Phys. **93**, 015005.

Bernevig, B. Andrei, and Taylor L. Hughes, 2013, *Topological Insulators and Topological Superconductors*, illustrated edition (Princeton University Press, Princeton, NJ).

Bernevig, B. Andrei, Taylor L. Hughes, and Shou-Cheng Zhang, 2006, "Quantum spin Hall effect and topological phase transition in HgTe quantum wells," Science **314**, 1757–1761.

Bernevig, B. Andrei, and Shou-Cheng Zhang, 2006, "Quantum Spin Hall Effect," Phys. Rev. Lett. **96**, 106802.

Berry, Michael V., 1984, "Quantal phase factors accompanying adiabatic changes," Proc. R. Soc. A **392**, 45–57.

Brendel, Christian, Vittorio Peano, Oskar Painter, and Florian Marquardt, 2018, "Snowflake phononic topological insulator at the nanoscale," Phys. Rev. B **97**, 020102(R).

Brendel, Christian, Vittorio Peano, Oskar J. Painter, and Florian Marquardt, 2017, "Pseudomagnetic fields for sound at the nanoscale," Proc. Natl. Acad. Sci. U.S.A. **114**, E3390–E3395.

Brouder, Christian, Gianluca Panati, Matteo Calandra, Christophe Mourougane, and Nicola Marzari, 2007, "Exponential Localization of Wannier Functions in Insulators," Phys. Rev. Lett. **98**, 046402.

Cha, Jinwoong, Kun Woo Kim, and Chiara Daraio, 2018, "Experimental realization of on-chip topological nanoelectromechanical metamaterials," Nature (London) **564**, 229–233.

Chaunsali, R., E. Kim, A. Thakkar, P. G. Kevrekidis, and J. Yang, 2017, "Demonstrating an *In Situ* Topological Band Transition in Cylindrical Granular Chains," Phys. Rev. Lett. **119**, 024301.

Chaunsali, Rajesh, Chun-Wei Chen, and Jinkyu Yang, 2018, "Subwavelength and directional control of flexural waves in zone-folding induced topological plates," Phys. Rev. B **97**, 054307.

Chaunsali, Rajesh, and Georgios Theocharis, 2019, "Self-induced topological transition in phononic crystals by nonlinearity management," Phys. Rev. B **100**, 014302.

Chaunsali, Rajesh, Haitao Xu, Jinkyu Yang, Panayotis G. Kevrekidis, and Georgios Theocharis, 2021, "Stability of topological edge states under strong nonlinear effects," Phys. Rev. B **103**, 024106.

Chen, Ze-Guo, and Ying Wu, 2016, "Tunable Topological Phononic Crystals," Phys. Rev. Appl. **5**, 054021.

Cheng, Xiaojun, Camille Jouvaud, Xiang Ni, S. Hossein Mousavi, Azriel Z. Genack, and Alexander B. Khanikaev, 2016, "Robust reconfigurable electromagnetic pathways within a photonic topological insulator," Nat. Mater. **15**, 542–548.

Cleland, Andrew N., 2003, *Foundations of Nanomechanics: From Solid-State Theory to Device Applications*, Advanced Texts in Physics (Springer, Berlin).

Clerk, A. A., K. W. Lehnert, P. Bertet, J. R. Petta, and Y. Nakamura, 2020, "Hybrid quantum systems with circuit quantum electrodynamics," Nat. Phys. **16**, 257–267.

Cooper, N. R., J. Dalibard, and I. B. Spielman, 2019, "Topological bands for ultracold atoms," Rev. Mod. Phys. **91**, 015005.

Darabi, Amir, and Michael J. Leamy, 2019, "Tunable Nonlinear Topological Insulator for Acoustic Waves," Phys. Rev. Appl. **12**, 044030.

Darabi, Amir, Xiang Ni, Michael Leamy, and Andrea Alù, 2020, "Reconfigurable Floquet elastodynamic topological insulator based on synthetic angular momentum bias," Sci. Adv. **6**, eaba8656.

Delaney, R. D., M. D. Urmey, S. Mittal, B. M. Brubaker, J. M. Kindem, P. S. Burns, C. A. Regal, and K. W. Lehnert, 2022, "Superconducting-qubit readout via low-backaction electro-optic transduction," Nature (London) **606**, 489–493.

del Pino, Javier, Jesse J. Slim, and Ewold Verhagen, 2022, "Non-Hermitian chiral phononics through optomechanically induced squeezing," Nature (London) **606**, 82–87.

Delplace, Pierre, J. B. Marston, and Antoine Venaille, 2017, "Topological origin of equatorial waves," Science **358**, 1075–1077.

Deng, Yuanchen, Hao Ge, Yuan Tian, Minghui Lu, and Yun Jing, 2017, "Observation of zone folding induced acoustic topological insulators and the role of spin-mixing defects," Phys. Rev. B **96**, 184305.

Ding, Yujiang, Yugui Peng, Yifan Zhu, Xudong Fan, Jing Yang, Bin Liang, Xuefeng Zhu, Xiangang Wan, and Jianchun Cheng, 2019, "Experimental Demonstration of Acoustic Chern Insulators," Phys. Rev. Lett. **122**, 014302.

Fan, Xiying, Tianzhi Xia, Huahui Qiu, Qicheng Zhang, and Chunyin Qiu, 2022, "Tracking Valley Topology with Synthetic Weyl Paths," Phys. Rev. Lett. **128**, 216403.

Faure, Frédéric, 2022, "Manifestation of the topological index formula in quantum waves and geophysical waves," arXiv:1901.10592.

Fleury, Romain, Alexander B. Khanikaev, and Andrea Alù, 2016, "Floquet topological insulators for sound," Nat. Commun. **7**, 11744.

Fruchart, Michel, Seung-Yeol Jeon, Kahyun Hur, Vadim Cheianov, Ulrich Wiesner, and Vincenzo Vitelli, 2018, "Soft self-assembly of

Weyl materials for light and sound," Proc. Natl. Acad. Sci. U.S.A. **115**, E3655–E3664.
Ge, Hao, Xu Ni, Yuan Tian, Samit Kumar Gupta, Ming-Hui Lu, Xin Lin, Wei-Dong Huang, C. T. Chan, and Yan-Feng Chen, 2018, "Experimental Observation of Acoustic Weyl Points and Topological Surface States," Phys. Rev. Appl. **10**, 014017.
Guinea, F., M. I. Katsnelson, and A. K. Geim, 2010, "Energy gaps and a zero-field quantum Hall effect in graphene by strain engineering," Nat. Phys. **6**, 30–33.
Habraken, S. J. M., K. Stannigel, M. D. Lukin, P. Zoller, and P. Rabl, 2012, "Continuous mode cooling and phonon routers for phononic quantum networks,"New J. Phys. **14**, 115004.
Hafezi, M., S. Mittal, J. Fan, A. Migdall, and J. M. Taylor, 2013, "Imaging topological edge states in silicon photonics," Nat. Photonics **7**, 1001–1005.
Hafezi, Mohammad, Eugene A. Demler, Mikhail D. Lukin, and Jacob M. Taylor, 2011, "Robust optical delay lines with topological protection," Nat. Phys. **7**, 907–912.
Haldane, F. D. M., 1988, "Model for a Quantum Hall Effect without Landau Levels: Condensed-Matter Realization of the 'Parity Anomaly,' " Phys. Rev. Lett. **61**, 2015–2018.
Haldane, F. D. M., and S. Raghu, 2008, "Possible Realization of Directional Optical Waveguides in Photonic Crystals with Broken Time-Reversal Symmetry," Phys. Rev. Lett. **100**, 013904.
Han, Xiangzhen, Yu-Gui Peng, Li Li, Yujin Hu, Chaosheng Mei, De-Gang Zhao, Xue-Feng Zhu, and Xuelin Wang, 2019, "Experimental Demonstration of Acoustic Valley Hall Topological Insulators with the Robust Selection of C_{3v}-Symmetric Scatterers," Phys. Rev. Appl. **12**, 014046.
Harari, Gal, Miguel A. Bandres, Yaakov Lumer, Mikael C. Rechtsman, Y. D. Chong, Mercedeh Khajavikhan, Demetrios N. Christodoulides, and Mordechai Segev, 2018, "Topological insulator laser: Theory," Science **359**, eaar4003.
Hasan, M. Z., and C. L. Kane, 2010, "Colloquium: Topological insulators," Rev. Mod. Phys. **82**, 3045–3067.
Hatsugai, Yasuhiro, 1993, "Chern Number and Edge States in the Integer Quantum Hall Effect," Phys. Rev. Lett. **71**, 3697–3700.
He, Cheng, Zheng Li, Xu Ni, Xiao-Chen Sun, Si-Yuan Yu, Ming-Hui Lu, Xiao-Ping Liu, and Yan-Feng Chen, 2016, "Topological phononic states of underwater sound based on coupled ring resonators," Appl. Phys. Lett. **108**, 031904.
He, Cheng, Xu Ni, Hao Ge, Xiao-Chen Sun, Yan-Bin Chen, Ming-Hui Lu, Xiao-Ping Liu, and Yan-Feng Chen, 2016, "Acoustic topological insulator and robust one-way sound transport," Nat. Phys. **12**, 1124–1129.
He, Hailong, Chunyin Qiu, Liping Ye, Xiangxi Cai, Xiying Fan, Manzhu Ke, Fan Zhang, and Zhengyou Liu, 2018, "Topological negative refraction of surface acoustic waves in a Weyl phononic crystal," Nature (London) **560**, 61–64.
Hofstadter, Douglas R., 1976, "Energy levels and wave functions of Bloch electrons in rational and irrational magnetic fields," Phys. Rev. B **14**, 2239–2249.
Huang, Hongbo, Jiujiu Chen, and Shaoyong Huo, 2021, "Recent advances in topological elastic metamaterials," J. Phys. Condens. Matter **33**, 503002.
Huber, Sebastian D., 2016, "Topological mechanics," Nat. Phys. **12**, 621–623.
Huo, Shao-yong, Jiu-jiu Chen, Hong-bo Huang, and Guo-liang Huang, 2017, "Simultaneous multi-band valley-protected topological edge states of shear vertical wave in two-dimensional phononic crystals with veins," Sci. Rep. **7**, 10335.
Jackiw, R., and C. Rebbi, 1976, "Solitons with fermion number 1/2," Phys. Rev. D **13**, 3398–3409.
Jaksch, D., and P. Zoller, 2003, "Creation of effective magnetic fields in optical lattices: The Hofstadter butterfly for cold neutral atoms," New J. Phys. **5**, 56–56.
Ju, Long, *et al.*, 2015, "Topological valley transport at bilayer graphene domain walls," Nature (London) **520**, 650–655.
Kane, C. L., and T. C. Lubensky, 2014, "Topological boundary modes in isostatic lattices," Nat. Phys. **10**, 39–45.
Kane, C. L., and E. J. Mele, 1997, "Size, Shape, and Low Energy Electronic Structure of Carbon Nanotubes," Phys. Rev. Lett. **78**, 1932–1935.
Kane, C. L., and E. J. Mele, 2005a, "Quantum Spin Hall Effect in Graphene," Phys. Rev. Lett. **95**, 226801.
Kane, C. L., and E. J. Mele, 2005b, "$Z2$ Topological Order and the Quantum Spin Hall Effect," Phys. Rev. Lett. **95**, 146802.
Kariyado, Toshikaze, and Yasuhiro Hatsugai, 2015, "Manipulation of Dirac cones in mechanical graphene," Sci. Rep. **5**, 18107.
Khanikaev, Alexander B., Romain Fleury, S. Hossein Mousavi, and Andrea Alù, 2015, "Topologically robust sound propagation in an angular-momentum-biased graphene-like resonator lattice," Nat. Commun. **6**, 8260.
Kittel, Charles, 2004, *Introduction to Solid State Physics*, 8th ed. (John Wiley & Sons, Hoboken, NJ).
Klitzing, K. v., G. Dorda, and M. Pepper, 1980, "New Method for High-Accuracy Determination of the Fine-Structure Constant Based on Quantized Hall Resistance," Phys. Rev. Lett. **45**, 494–497.
Kohmoto, M., 1985, "Topological invariant and the quantization of the Hall conductance," Ann. Phys. (N.Y.) **160**, 343–354.
König, Markus, Steffen Wiedmann, Christoph Brüne, Andreas Roth, Hartmut Buhmann, Laurens W. Molenkamp, Xiao-Liang Qi, and Shou-Cheng Zhang, 2007, "Quantum spin Hall insulator state in HgTe quantum wells," Science **318**, 766–770.
Landau, L. D., and E. M. Lifshitz, 1981, *Quantum Mechanics: Non-relativistic Theory* (Elsevier, New York).
Laughlin, R. B., 1981, "Quantized Hall conductivity in two dimensions," Phys. Rev. B **23**, 5632–5633.
Lemonde, Marc-Antoine, Vittorio Peano, Peter Rabl, and Dimitris G. Angelakis, 2019, "Quantum state transfer via acoustic edge states in a 2D optomechanical array," New J. Phys. **21**, 113030.
Levy, N., S. A. Burke, K. L. Meaker, M. Panlasigui, A. Zettl, F. Guinea, A. H. Castro Neto, and M. F. Crommie, 2010, "Strain-induced pseudo-magnetic fields greater than 300 tesla in graphene nanobubbles," Science **329**, 544–547.
Leykam, Daniel, and Y. D. Chong, 2016, "Edge Solitons in Nonlinear-Photonic Topological Insulators," Phys. Rev. Lett. **117**, 143901.
Li, Feng, Xueqin Huang, Jiuyang Lu, Jiahong Ma, and Zhengyou Liu, 2018, "Weyl points and Fermi arcs in a chiral phononic crystal," Nat. Phys. **14**, 30–34.
Li, Tracy, Lucia Duca, Martin Reitter, Fabian Grusdt, Eugene Demler, Manuel Endres, Monika Schleier-Smith, Immanuel Bloch, and Ulrich Schneider, 2016, "Bloch state tomography using Wilson lines," Science **352**, 1094–1097.
Liang, G. Q., and Y. D. Chong, 2013, "Optical Resonator Analog of a Two-Dimensional Topological Insulator," Phys. Rev. Lett. **110**, 203904.
Liu, Yizhou, Xiaobin Chen, and Yong Xu, 2020, "Topological Phononics: From Fundamental Models to Real Materials," Adv. Funct. Mater. **30**, 1904784.
Lu, Jiuyang, Chunyin Qiu, Weiyin Deng, Xueqin Huang, Feng Li, Fan Zhang, Shuqi Chen, and Zhengyou Liu, 2018, "Valley Topological Phases in Bilayer Sonic Crystals," Phys. Rev. Lett. **120**, 116802.

Lu, Jiuyang, Chunyin Qiu, Liping Ye, Xiying Fan, Manzhu Ke, Fan Zhang, and Zhengyou Liu, 2017, "Observation of topological valley transport of sound in sonic crystals," Nat. Phys. **13**, 369–374.

Lu, Ling, John D. Joannopoulos, and Marin Soljačić, 2014, "Topological photonics," Nat. Photonics **8**, 821–829.

Lumer, Yaakov, Yonatan Plotnik, Mikael C. Rechtsman, and Mordechai Segev, 2013, "Self-Localized States in Photonic Topological Insulators," Phys. Rev. Lett. **111**, 243905.

Ma, Guancong, Meng Xiao, and C. T. Chan, 2019, "Topological phases in acoustic and mechanical systems," Nat. Rev. Phys. **1**, 281–294.

Ma, Jingwen, Xiang Xi, Yuan Li, and Xiankai Sun, 2021, "Nanomechanical topological insulators with an auxiliary orbital degree of freedom," Nat. Nanotechnol. **16**, 576–583.

Ma, Jingwen, Xiang Xi, and Xiankai Sun, 2021, "Experimental demonstration of dual-band nano-electromechanical valley-Hall topological metamaterials," Adv. Mater. **33**, 2006521.

MacCabe, Gregory S., Hengjiang Ren, Jie Luo, Justin D. Cohen, Hengyun Zhou, Alp Sipahigil, Mohammad Mirhosseini, and Oskar Painter, 2020, "Nano-acoustic resonator with ultralong phonon lifetime," Science **370**, 840–843.

Mañes, J. L., 2007, "Symmetry-based approach to electron-phonon interactions in graphene," Phys. Rev. B **76**, 045430.

Marconcini, P., and M. Macucci, 2011, "The $k \cdot p$ method and its application to graphene, carbon nanotubes and graphene nanoribbons: The Dirac equation," Riv. Nuovo Cimento **34**, 489–584.

Martin, Ivar, Ya. M. Blanter, and A. F. Morpurgo, 2008, "Topological Confinement in Bilayer Graphene," Phys. Rev. Lett. **100**, 036804.

Mathew, John P., Javier del Pino, and Ewold Verhagen, 2020, "Synthetic gauge fields for phonon transport in a nano-optomechanical system," Nat. Nanotechnol. **15**, 198–202.

Matlack, Kathryn H., Marc Serra-Garcia, Antonio Palermo, Sebastian D. Huber, and Chiara Daraio, 2018, "Designing perturbative metamaterials from discrete models," Nat. Mater. **17**, 323–328.

Mei, Jun, Ze-Guo Chen, and Ying Wu, 2016, "Pseudo-time-reversal symmetry and topological edge states in two-dimensional acoustic crystals," Sci. Rep. **6**, 32752.

Mei, Jun, Jiqian Wang, Xiujuan Zhang, Siyuan Yu, Zhen Wang, and Ming-Hui Lu, 2019, "Robust and High-Capacity Phononic Communications through Topological Edge States by Discrete Degree-of-Freedom Multiplexing," Phys. Rev. Appl. **12**, 054041.

Mermin, N. D., 1979, "The topological theory of defects in ordered media," Rev. Mod. Phys. **51**, 591–648.

Miniaci, M., and R. K. Pal, 2021, "Design of topological elastic waveguides," J. Appl. Phys. **130**, 141101.

Miniaci, M., R. K. Pal, B. Morvan, and M. Ruzzene, 2018, "Experimental Observation of Topologically Protected Helical Edge Modes in Patterned Elastic Plates," Phys. Rev. X **8**, 031074.

Mitchell, Noah P., Lisa M. Nash, Daniel Hexner, Ari M. Turner, and William T. M. Irvine, 2018, "Amorphous topological insulators constructed from random point sets," Nat. Phys. **14**, 380–385.

Mittal, Sunil, Gregory Moille, Kartik Srinivasan, Yanne K. Chembo, and Mohammad Hafezi, 2021, "Topological frequency combs and nested temporal solitons," Nat. Phys. **17**, 1169–1176.

Mousavi, S. Hossein, Alexander B. Khanikaev, and Zheng Wang, 2015, "Topologically protected elastic waves in phononic metamaterials," Nat. Commun. **6**, 8682.

Mukherjee, Sebabrata, and Mikael C. Rechtsman, 2020, "Observation of Floquet solitons in a topological bandgap," Science **368**, 856–859.

Nash, Lisa M., Dustin Kleckner, Alismari Read, Vincenzo Vitelli, Ari M. Turner, and William T. M. Irvine, 2015, "Topological mechanics of gyroscopic metamaterials," Proc. Natl. Acad. Sci. U.S.A. **112**, 14495–14500.

Nassar, Hussein, Behrooz Yousefzadeh, Romain Fleury, Massimo Ruzzene, Andrea Alù, Chiara Daraio, Andrew N. Norris, Guoliang Huang, and Michael R. Haberman, 2020, "Nonreciprocity in acoustic and elastic materials," Nat. Rev. Mater. **5**, 667–685.

Ni, Xu, Cheng He, Xiao-Chen Sun, Xiao-ping Liu, Ming-Hui Lu, Liang Feng, and Yan-Feng Chen, 2015, "Topologically protected one-way edge mode in networks of acoustic resonators with circulating air flow," New J. Phys. **17**, 053016.

Nii, Y., and Y. Onose, 2023, "Imaging an Acoustic Topological Edge Mode on a Patterned Substrate with Microwave Impedance Microscopy," Phys. Rev. Appl. **19**, 014001.

Nomura, T., X.-X. Zhang, S. Zherlitsyn, J. Wosnitza, Y. Tokura, N. Nagaosa, and S. Seki, 2019, "Phonon Magnetochiral Effect," Phys. Rev. Lett. **122**, 145901.

Ohgushi, Kenya, Shuichi Murakami, and Naoto Nagaosa, 2000, "Spin anisotropy and quantum Hall effect in the Kagomé lattice: Chiral spin state based on a ferromagnet," Phys. Rev. B **62**, R6065–R6068.

Ozawa, Tomoki, *et al.*, 2019, "Topological photonics," Rev. Mod. Phys. **91**, 015006.

Pal, Raj Kumar, and Massimo Ruzzene, 2017, "Edge waves in plates with resonators: An elastic analogue of the quantum valley Hall effect," New J. Phys. **19**, 025001.

Pal, Raj Kumar, Marshall Schaeffer, and Massimo Ruzzene, 2016, "Helical edge states and topological phase transitions in phononic systems using bi-layered lattices," J. Appl. Phys. **119**, 084305.

Pal, Raj Kumar, Javier Vila, Michael Leamy, and Massimo Ruzzene, 2018, "Amplitude-dependent topological edge states in nonlinear phononic lattices," Phys. Rev. E **97**, 032209.

Peano, V., C. Brendel, M. Schmidt, and F. Marquardt, 2015, "Topological Phases of Sound and Light," Phys. Rev. X **5**, 031011.

Peano, Vittorio, Martin Houde, Florian Marquardt, and Aashish A. Clerk, 2016, "Topological Quantum Fluctuations and Traveling Wave Amplifiers," Phys. Rev. X **6**, 041026.

Peano, Vittorio, Florian Sapper, and Florian Marquardt, 2021, "Rapid Exploration of Topological Band Structures Using Deep Learning," Phys. Rev. X **11**, 021052.

Peng, Yu-Gui, Cheng-Zhi Qin, De-Gang Zhao, Ya-Xi Shen, Xiang-Yuan Xu, Ming Bao, Han Jia, and Xue-Feng Zhu, 2016, "Experimental demonstration of anomalous Floquet topological insulator for sound," Nat. Commun. **7**, 13368.

Pilozzi, Laura, Francis A. Farrelly, Giulia Marcucci, and Claudio Conti, 2018, "Machine learning inverse problem for topological photonics," Commun. Phys. **1**, 57.

Prodan, E., and H. Schulz-Baldes, 2016, *Bulk and Boundary Invariants for Complex Topological Insulators: From K-Theory to Physics* (Springer International Publishing, Cham, Switzerland).

Prodan, Emil, and Camelia Prodan, 2009, "Topological Phonon Modes and Their Role in Dynamic Instability of Microtubules," Phys. Rev. Lett. **103**, 248101.

Qin, Hong, and Yichen Fu, 2023, "Topological Langmuir-cyclotron wave," Sci. Adv. **9**, eadd8041.

Qin, Tao, Jianhui Zhou, and Junren Shi, 2012, "Berry curvature and the phonon Hall effect," Phys. Rev. B **86**, 104305.

Ren, Hengjiang, Tirth Shah, Hannes Pfeifer, Christian Brendel, Vittorio Peano, Florian Marquardt, and Oskar Painter, 2022, "Topological phonon transport in an optomechanical system," Nat. Commun. **13**, 3476.

Safavi-Naeini, Amir H., Dries Van Thourhout, Roel Baets, and Raphaël Van Laer, 2019, "Controlling phonons and photons at the

wavelength scale: Integrated photonics meets integrated phononics," Optica **6**, 213.
Salerno, Grazia, Tomoki Ozawa, Hannah M. Price, and Iacopo Carusotto, 2016, "Floquet topological system based on frequency-modulated classical coupled harmonic oscillators," Phys. Rev. B **93**, 085105.
Sanavio, Claudio, Vittorio Peano, and André Xuereb, 2020, "Nonreciprocal topological phononics in optomechanical arrays," Phys. Rev. B **101**, 085108.
Semenoff, Gordon W., 1984, "Condensed-Matter Simulation of a Three-Dimensional Anomaly," Phys. Rev. Lett. **53**, 2449–2452.
Serra-Garcia, Marc, Valerio Peri, Roman Süsstrunk, Osama R. Bilal, Tom Larsen, Luis Guillermo Villanueva, and Sebastian D. Huber, 2018, "Observation of a phononic quadrupole topological insulator," Nature (London) **555**, 342 EP-.
Shah, Tirth, Florian Marquardt, and Vittorio Peano, 2021, "Tunneling in the Brillouin zone: Theory of backscattering in valley Hall edge channels," Phys. Rev. B **104**, 235431.
Shen, Yuanyuan, Chunyin Qiu, Xiangxi Cai, Liping Ye, Jiuyang Lu, Manzhu Ke, and Zhengyou Liu, 2019, "Valley-projected edge modes observed in underwater sonic crystals," Appl. Phys. Lett. **114**, 023501.
Simon, Barry, 1983, "Holonomy, the Quantum Adiabatic Theorem, and Berry's Phase," Phys. Rev. Lett. **51**, 2167–2170.
Smirnova, Daria, Daniel Leykam, Yidong Chong, and Yuri Kivshar, 2020, "Nonlinear topological photonics," Appl. Phys. Rev. **7**, 021306.
Souslov, Anton, Benjamin C. van Zuiden, Denis Bartolo, and Vincenzo Vitelli, 2017, "Topological sound in active-liquid metamaterials," Nat. Phys. **13**, 1091–1094.
Strohm, C., G. L. J. A. Rikken, and P. Wyder, 2005, "Phenomenological Evidence for the Phonon Hall Effect," Phys. Rev. Lett. **95**, 155901.
Süsstrunk, Roman, and Sebastian D. Huber, 2015, "Observation of phononic helical edge states in a mechanical topological insulator," Science **349**, 47–50.
Süsstrunk, Roman, and Sebastian D. Huber, 2016, "Classification of topological phonons in linear mechanical metamaterials," Proc. Natl. Acad. Sci. U.S.A. **113**, E4767–E4775.
Süsstrunk, Roman, Philipp Zimmermann, and Sebastian D Huber, 2017, "Switchable topological phonon channels," New J. Phys. **19**, 015013.
Thouless, D. J., M. Kohmoto, M. P. Nightingale, and M. den Nijs, 1982, "Quantized Hall Conductance in a Two-Dimensional Periodic Potential," Phys. Rev. Lett. **49**, 405–408.
Tian, Zhenhua, Chen Shen, Junfei Li, Eric Reit, Hunter Bachman, Joshua E. S. Socolar, Steven A. Cummer, and Tony Jun Huang, 2020, "Dispersion tuning and route reconfiguration of acoustic waves in valley topological phononic crystals," Nat. Commun. **11**, 762.
Tsaturyan, Y., A. Barg, E. S. Polzik, and A. Schliesser, 2017, "Ultracoherent nanomechanical resonators via soft clamping and dissipation dilution," Nat. Nanotechnol. **12**, 776–783.
Vila, Javier, Raj Kumar Pal, and Massimo Ruzzene, 2017, "Observation of topological valley modes in an elastic hexagonal lattice," Phys. Rev. B **96**, 134307.
Wan, Xiangang, Ari M. Turner, Ashvin Vishwanath, and Sergey Y. Savrasov, 2011, "Topological semimetal and Fermi-arc surface states in the electronic structure of pyrochlore iridates," Phys. Rev. B **83**, 205101.
Wang, Ji-Qian, *et al.*, 2022, "Extended topological valley-locked surface acoustic waves," Nat. Commun. **13**, 1324.
Wang, Mudi, Liping Ye, J. Christensen, and Zhengyou Liu, 2018, "Valley Physics in Non-Hermitian Artificial Acoustic Boron Nitride," Phys. Rev. Lett. **120**, 246601.
Wang, Mudi, Wenyi Zhou, Liya Bi, Chunyin Qiu, Manzhu Ke, and Zhengyou Liu, 2020, "Valley-locked waveguide transport in acoustic heterostructures," Nat. Commun. **11**, 3000.
Wang, Pai, Ling Lu, and Katia Bertoldi, 2015, "Topological Phononic Crystals with One-Way Elastic Edge Waves," Phys. Rev. Lett. **115**, 104302.
Wang, Yao-Ting, Pi-Gang Luan, and Shuang Zhang, 2015, "Coriolis force induced topological order for classical mechanical vibrations," New J. Phys. **17**, 073031.
Wang, Yao-Ting, and Ya-Wen Tsai, 2018, "Multiple Weyl and double-Weyl points in an elastic chiral lattice," New J. Phys. **20**, 083031.
Wang, Zheng, Yidong Chong, J. D. Joannopoulos, and Marin Soljačić, 2009, "Observation of unidirectional backscattering-immune topological electromagnetic states," Nature (London) **461**, 772–775.
Wen, Xinhua, Chunyin Qiu, Jiuyang Lu, Hailong He, Manzhu Ke, and Zhengyou Liu, 2018, "Acoustic Dirac degeneracy and topological phase transitions realized by rotating scatterers," J. Appl. Phys. **123**, 091703.
Wen, Xinhua, Chunyin Qiu, Yajuan Qi, Liping Ye, Manzhu Ke, Fan Zhang, and Zhengyou Liu, 2019, "Acoustic Landau quantization and quantum-Hall-like edge states," Nat. Phys. **15**, 352–356.
Wu, Long-Hua, and Xiao Hu, 2015, "Scheme for Achieving a Topological Photonic Crystal by Using Dielectric Material," Phys. Rev. Lett. **114**, 223901.
Xi, Xiang, Jingwen Ma, Shuai Wan, Chun-Hua Dong, and Xiankai Sun, 2021, "Observation of chiral edge states in gapped nanomechanical graphene," Sci. Adv. **7**, eabe1398.
Xia, Bai-Zhan, Sheng-Jie Zheng, Ting-Ting Liu, Jun-Rui Jiao, Ning Chen, Hong-Qing Dai, De-Jie Yu, and Jian Liu, 2018, "Observation of valleylike edge states of sound at a momentum away from the high-symmetry points," Phys. Rev. B **97**, 155124.
Xiao, Meng, Wen-Jie Chen, Wen-Yu He, and C. T. Chan, 2015, "Synthetic gauge flux and Weyl points in acoustic systems," Nat. Phys. **11**, 920–924.
Xiao, Meng, Guancong Ma, Zhiyu Yang, Ping Sheng, Z. Q. Zhang, and C. T. Chan, 2015, "Geometric phase and band inversion in periodic acoustic systems," Nat. Phys. **11**, 240–244.
Xu, H., D. Mason, Luyao Jiang, and J. G. E. Harris, 2016, "Topological energy transfer in an optomechanical system with exceptional points," Nature (London) **537**, 80–83.
Xu, Mingran, Kei Yamamoto, Jorge Puebla, Korbinian Baumgaertl, Bivas Rana, Katsuya Miura, Hiromasa Takahashi, Dirk Grundler, Sadamichi Maekawa, and Yoshichika Otani, 2020, "Nonreciprocal surface acoustic wave propagation via magneto-rotation coupling," Sci. Adv. **6**, eabb1724.
Yang, Yahui, Zhaoju Yang, and Baile Zhang, 2018, "Acoustic valley edge states in a graphene-like resonator system," J. Appl. Phys. **123**, 091713.
Yang, Zhaoju, Fei Gao, Xihang Shi, Xiao Lin, Zhen Gao, Yidong Chong, and Baile Zhang, 2015, "Topological Acoustics," Phys. Rev. Lett. **114**, 114301.
Yang, Zhaoju, and Baile Zhang, 2016, "Acoustic Type-II Weyl Nodes from Stacking Dimerized Chains," Phys. Rev. Lett. **117**, 224301.
Yu, Si-Yuan, Cheng He, Xiao-Chen Sun, Hong-Fei Wang, Ji-Qian Wang, Zi-Dong Zhang, Bi-Ye Xie, Yuan Tian, Ming-Hui Lu, and

Yan-Feng Chen, 2021, "Critical couplings in topological-insulator waveguide-resonator systems observed in elastic waves," Natl. Sci. Rev. **8**, nwaa262.

Yu, Si-Yuan, Cheng He, Zhen Wang, Fu-Kang Liu, Xiao-Chen Sun, Zheng Li, Hai-Zhou Lu, Ming-Hui Lu, Xiao-Ping Liu, and Yan-Feng Chen, 2018, "Elastic pseudospin transport for integratable topological phononic circuits," Nat. Commun. **9**, 3072.

Yves, Simon, Romain Fleury, Fabrice Lemoult, Mathias Fink, and Geoffroy Lerosey, 2017, "Topological acoustic polaritons: Robust sound manipulation at the subwavelength scale," New J. Phys. **19**, 075003.

Zhang, Fan, Allan H. MacDonald, and Eugene J. Mele, 2013, "Valley Chern numbers and boundary modes in gapped bilayer graphene," Proc. Natl. Acad. Sci. U.S.A. **110**, 10546–10551.

Zhang, Lifa, and Qian Niu, 2015, "Chiral Phonons at High-Symmetry Points in Monolayer Hexagonal Lattices," Phys. Rev. Lett. **115**, 115502.

Zhang, Lifa, Jie Ren, Jian-Sheng Wang, and Baowen Li, 2010, "Topological Nature of the Phonon Hall Effect," Phys. Rev. Lett. **105**, 225901.

Zhang, Qicheng, *et al.*, 2022, "Gigahertz topological valley Hall effect in nanoelectromechanical phononic crystals," Nat. Electron. **5**, 157–163.

Zhang, Xiujuan, Meng Xiao, Ying Cheng, Ming-Hui Lu, and Johan Christensen, 2018, "Topological sound," Commun. Phys. **1**, 97.

Zhang, Zhiwang, Ye Tian, Ying Cheng, Qi Wei, Xiaojun Liu, and Johan Christensen, 2018, "Topological Acoustic Delay Line," Phys. Rev. Appl. **9**, 034032.

Zhang, Zhiwang, Ye Tian, Yihe Wang, Shuxiang Gao, Ying Cheng, Xiaojun Liu, and Johan Christensen, 2018, "Directional acoustic antennas based on valley-Hall topological insulators," Adv. Mater. **30**, 1803229.

Zhang, Zhiwang, Qi Wei, Ying Cheng, Ting Zhang, Dajian Wu, and Xiaojun Liu, 2017, "Topological Creation of Acoustic Pseudospin Multipoles in a Flow-Free Symmetry-Broken Metamaterial Lattice," Phys. Rev. Lett. **118**, 084303.

Zhang, Zi-Dong, Si-Yuan Yu, Hao Ge, Ji-Qian Wang, Hong-Fei Wang, Kang-Fu Liu, Tao Wu, Cheng He, Ming-Hui Lu, and Yan-Feng Chen, 2021, "Topological Surface Acoustic Waves," Phys. Rev. Appl. **16**, 044008.

Zhao, Han, Xingdu Qiao, Tianwei Wu, Bikashkali Midya, Stefano Longhi, and Liang Feng, 2019, "Non-Hermitian topological light steering," Science **365**, 1163–1166.

Zhu, Hanyu, Jun Yi, Ming-Yang Li, Jun Xiao, Lifa Zhang, Chih-Wen Yang, Robert A. Kaindl, Lain-Jong Li, Yuan Wang, and Xiang Zhang, 2018, "Observation of chiral phonons," Science **359**, 579–582.

Zhu, Hongfei, Ting-Wei Liu, and Fabio Semperlotti, 2018, "Design and experimental observation of valley-Hall edge states in diatomic-graphene-like elastic waveguides," Phys. Rev. B **97**, 174301.